

Bagged filters for partially observed interacting systems

Edward L. Ionides*

Department of Statistics, University of Michigan
Kidus Asfaw

Department of Statistics, University of Michigan
Joonha Park

Department of Mathematics, University of Kansas
Aaron A. King

Department of Ecology and Evolutionary Biology &
Center for the Study of Complex Systems, University of Michigan

Abstract

Bagging (i.e., bootstrap aggregating) involves combining an ensemble of bootstrap estimators. We consider bagging for inference from noisy or incomplete measurements on a collection of interacting stochastic dynamic systems. Each system is called a unit, and each unit is associated with a spatial location. A motivating example arises in epidemiology, where each unit is a city: the majority of transmission occurs within a city, with smaller yet epidemiologically important interactions arising from disease transmission between cities. Monte Carlo filtering methods used for inference on nonlinear non-Gaussian systems can suffer from a curse of dimensionality as the number of units increases. We introduce bagged filter (BF) methodology which combines an ensemble of Monte Carlo filters, using spatiotemporally localized weights to select successful filters at each unit and time. We obtain conditions under which likelihood evaluation using a BF algorithm can beat a curse of dimensionality, and we demonstrate applicability even when these conditions do not hold. BF can out-perform an ensemble Kalman filter on a coupled population dynamics model describing infectious disease transmission. A block particle filter also performs well on this task, though the bagged filter respects smoothness and conservation laws that a block particle filter can violate.

Keywords: Particle filter; Sequential Monte Carlo; Markov process; Population dynamics

*This work was supported by National Science Foundation grants DMS-1761603 and DMS-1646108, and National Institutes of Health grants 1-U54-GM111274 and 1-U01-GM110712.

1 Introduction

Bagging is a technique to improve numerically unstable estimators by combining an ensemble of replicated bootstrap calculations (Breiman, 1996). In the context of nonlinear partially observed dynamic systems, the bootstrap filter of Gordon et al. (1993) has led to a variety of particle filter (PF) methodologies (Doucet et al., 2001; Doucet and Johansen, 2011); Here, we consider algorithms combining an ensemble of replicated particle filters, which we term *bagged filter* algorithms. Standard PF methods suffer from a curse of dimensionality (COD), defined as an exponential increase in computational requirement as the problem size grows, limiting its applicability to large systems (Bengtsson et al., 2008; Snyder et al., 2015; Rebeschini and van Handel, 2015). The COD presents empirically as numerical instability of the Monte Carlo algorithm for affordable numbers of particles. Much previous research has investigated scalable approaches to filtering and inference with applications to spatiotemporal systems. Our bagged filters are in the class of *plug-and-play* algorithms, meaning that they require as input a simulator for the latent dynamic process but not an evaluator of transition probabilities (Bretó et al., 2009; He et al., 2010). This simulation-based approach, also known as *likelihood-free* (Brehmer et al., 2020) or *equation-free* (Kevrekidis and Samaey, 2009), facilitates application to a wide class of models. The ensemble Kalman filter (Evensen and van Leeuwen, 1996; Lei et al., 2010; Katzfuss et al., 2020) is a widely used plug-and-play method which uses simulations to construct a nonlinear filter that is exact for a linear Gaussian model. Another plug-and-play approach to combat the COD is the block particle filter (Rebeschini and van Handel, 2015; Ng et al., 2002). Both ensemble Kalman filter and block particle filter methods construct trajectories that can violate smoothness and conservation properties of the dynamic model. By contrast, our bagged filters are built using valid trajectories of the dynamic model, making localization approximations only when comparing these trajectories to data.

The replicated stochastic trajectories in a bagged filter form an ensemble of representations of the dynamic system. Unlike the particles in a particle filter or ensemble Kalman filter, the bagged replicates are independent in a Monte Carlo sense. Bagged filters therefore

bear some resemblance to *poor man’s ensemble* forecasting methodology in which a collection of independently constructed forecasts is generated using different models and methods (Ebert, 2001). Poor man’s ensembles have sometimes been found to have greater forecasting skill than any one forecast (Leutbecher and Palmer, 2008; Palmer, 2002; Chandler, 2013). One explanation for this phenomenon is that even a hypothetically perfect model cannot provide effective filtering using methodology afflicted by the COD. We show that bagged filter methodology can relieve this limitation. From this perspective, the independence of the forecasts in the poor man’s ensemble, rather than the diversity of model structures, may be the key to its success.

We first consider a simple bagged filter where each replicate is an independent simulation of the latent process model. We call this the unadapted bagged filter (UBF) since the replicates in the ensemble depend on the model but not on the data. UBF is described in Sec. 2, with a theoretical analysis presented in Sec. 2.1. Each UBF replicate corresponds to a basic PF algorithm with a single particle. We show that UBF formally beats the COD under a weak mixing assumption, though UBF can have poor numerical behavior if a very large number of replicates are needed to reach this happy asymptotic limit. Subsequent empirical results show that UBF may nevertheless be a useful algorithm in some situations. In Sec. 3, we generalize UBF to construct an adapted bagged filter (ABF) where each replicate tracks the data. The price of adaptation is that ABF no longer fully avoids the COD, a limitation that can be controlled in certain situations by supplementing ABF with a technique called intermediate resampling, to obtain the ABF-IR algorithm. Theoretical results for ABF and ABF-IR algorithms are developed in Sec. 3.1. The algorithms are demonstrated in action and compared with alternative approaches in Sec. 4.

2 The unadapted bagged filter (UBF)

Suppose the collection of units is indexed by the set $\{1, 2, \dots, U\}$, which is written as $1:U$. The latent Markov process is denoted by $\{\mathbf{X}_n, n \in 0:N\}$, with $\mathbf{X}_n = X_{1:U,n}$ taking values in a product space \mathbb{X}^U . This discrete time process may arise from a continuous time Markov

process $\{\mathbf{X}(t), t_0 \leq t \leq t_N\}$ observed at times $t_{1:N}$, and in this case we set $\mathbf{X}_n = \mathbf{X}(t_n)$. The initial value \mathbf{X}_0 may be stochastic or deterministic. Observations are made on each unit, modeled by an observable process $\{\mathbf{Y}_n = Y_{1:U,n}, n \in 1:N\}$ which takes values in a product space \mathbb{Y}^U . Observations are modeled as being conditionally independent given the latent process. The conditional independence of measurements applies over both time and the unit structure, so the collection $\{Y_{u,n}, u \in 1:U, n \in 1:N\}$ is conditionally independent given $\{X_{u,n}, u \in 1:U, n \in 1:N\}$. The unit structure for the observation process is not necessary for all that follows (see Sec. S1). We suppose the existence of a joint density $f_{\mathbf{X}_{0:N}, \mathbf{Y}_{1:N}}$ of $X_{1:U,1:N}$ and $Y_{1:U,1:N}$ with respect to some appropriate measure, following a notational convention that the subscripts of f denote the joint or conditional density under consideration. The data are $y_{u,n}^*$ for unit u at time n . This model is a special case of a partially observed Markov process (POMP, Bretó et al., 2009), also known as a state space model or hidden Markov model. The additional unit structure, not generally required for a POMP, is appropriate for modeling interactions between units characterized by a spatial location, and so we call the model a SpatPOMP. In the following, we use a lexicographical ordering on the set of observations; Specifically, we define the set of observations preceding unit u at time n as

$$A_{u,n} = \{(\tilde{u}, \tilde{n}) : 1 \leq \tilde{n} < n \text{ or } (\tilde{n} = n \text{ and } \tilde{u} < u)\}. \quad (1)$$

The ordering of the spatial locations in (1) might seem artificial, and indeed densities such as $f_{X_{u,n}|X_{A_{u,n}}}$ will frequently be hard to compute or simulate from. The bagged filter algorithms we study do not evaluate or simulate such transition densities but only compute the measurement model on neighborhoods, unlike the filter of Beskos et al. (2017) built on a similar factorization. If sufficiently distant units are approximately independent, we say the system is *weakly coupled*. In this case, we suppose there is a neighborhood $B_{u,n} \subset A_{u,n}$ such that the latent process on $A_{u,n} \setminus B_{u,n}$ is approximately conditionally independent of $X_{u,n}$ given data on $B_{u,n}$.

Our primary interest is estimation of the log likelihood for the data given the model, $\ell = \log f_{\mathbf{Y}_{1:N}}(\mathbf{y}_{1:N}^*)$, which is of fundamental importance in both Bayesian and non-Bayesian

statistical inference. A general filtering problem is to evaluate $\mathbb{E}[h(X_{u,n}) | Y_{A_{u,n}} = y_{A_{u,n}}^*]$ for some function $h : \mathbb{X} \rightarrow \mathbb{R}$. Taking $h(x) = f_{Y_{u,n}|X_{u,n}}(y_{u,n}^* | x)$ gives a filtering representation of the likelihood evaluation problem. Further discussion on bagged filtering for other filtering problems is given in Sec. S10. For likelihood-based inference, maximization plays an important role in point estimation, confidence interval construction, hypothesis testing and model selection. An extension of bagged filtering to likelihood maximization is demonstrated in Sec. 4.3 following the approach described in Sec. S11.

Pseudocode for a UBF algorithm for likelihood evaluation is given below. The prediction weight $w_{u,n,i}^P$ gives an appropriate weighting for replicate i for predicting $y_{u,n}^*$ based on the most relevant data, $y_{B_{u,n}}^*$. Conditional log likelihoods are estimated using an approximation

$$\begin{aligned} \ell_{u,n} &= \log f_{Y_{u,n}|Y_{A_{u,n}}}(y_{u,n}^* | y_{A_{u,n}}^*) = \log \left(\int f_{Y_{u,n}|X_{u,n}}(y_{u,n}^* | x) f_{X_{u,n}|Y_{A_{u,n}}}(x | y_{A_{u,n}}^*) dx \right) \\ &\approx \log \left(\int f_{Y_{u,n}|X_{u,n}}(y_{u,n}^* | x) f_{X_{u,n}|Y_{B_{u,n}}}(x | y_{B_{u,n}}^*) dx \right). \end{aligned}$$

The choice of $B_{u,n}$ is determined empirically, with a bias-variance trade-off used to compare small neighborhoods such as $B_{u,n} = \{(u, n-1), (u-1, n)\}$ or $B_{u,n} = \{(u, n-1), (u, n-2)\}$ against larger neighborhoods. The plug-and-play property is evident because UBF requires as input a simulator for the latent coupled dynamic process but not an evaluator of transition probabilities. The pseudocode for UBF adopts a convention that implicit loops are carried out over all free indices, meaning indices with values that are not explicitly specified. For example, the construction of $w_{u,n,i}^P$ in UBF has an implicit loop over u , n and i . However, the summation constructing $\ell_{u,n}^{\text{MC}}$ does not have an implicit loop over i since the summation index i is specified explicitly and so is not a free index.

UBF. Unadapted bagged filter.

input:simulator for $f_{\mathbf{X}_0}(\mathbf{x}_0)$ and $f_{\mathbf{X}_n|\mathbf{X}_{n-1}}(\mathbf{x}_n | \mathbf{x}_{n-1})$ evaluator for $f_{Y_{u,n}|X_{u,n}}(y_{u,n} | x_{u,n})$ number of replicates, \mathcal{I} neighborhood structure, $B_{u,n}$ data, \mathbf{y}_n^* **implicit loops:** u in $1:U$, n in $1:N$, i in $1:\mathcal{I}$ **algorithm:**simulate $\mathbf{X}_{0:N,i} \sim f_{\mathbf{X}_{0:N}}(\mathbf{x}_{0:N})$ measurement weights, $w_{u,n,i}^M = f_{Y_{u,n}|X_{u,n}}(y_{u,n}^* | X_{u,n,i})$ prediction weights, $w_{u,n,i}^P = \prod_{(\tilde{u},\tilde{n}) \in B_{u,n}} w_{\tilde{u},\tilde{n},i}^M$ $\ell_{u,n}^{\text{MC}} = \log \left(\sum_{i=1}^{\mathcal{I}} w_{u,n,i}^M w_{u,n,i}^P \right) - \log \left(\sum_{i=1}^{\mathcal{I}} w_{u,n,i}^P \right)$ **output:**log likelihood estimate, $\ell^{\text{MC}} = \sum_{n=1}^N \sum_{u=1}^U \ell_{u,n}^{\text{MC}}$

2.1 UBF theory

A dataset $\mathbf{y}_{1:N}^*$ with U units is modeled via a joint density $f_{\mathbf{X}_{0:N}, \mathbf{Y}_{1:N}}$. We consider non-asymptotic bounds that apply for all values of U and N . To impose a requirement that distant regions of space-time behave similarly and have only weak dependence, we assert the following conditions which define constants ϵ_{A1} , ϵ_{A4} and Q used to bound the bias and variance in Theorem 1. Stronger bounds are obtained when the conditions hold for small ϵ_{A1} , ϵ_{A4} and Q .

Assumption A1. *There is an $\epsilon_{A1} > 0$, independent of U and N , and a collection of neighborhoods $\{B_{u,n} \subset A_{u,n}, u \in 1:U, n \in 1:N\}$ such that, for all u and n , any bounded real-valued*

function $|h(x)| \leq 1$, and any value of $x_{B_{u,n}^c}$,

$$\left| \int h(x_{u,n}) f_{X_{u,n}|Y_{B_{u,n}}, X_{B_{u,n}^c}}(x_{u,n} | y_{B_{u,n}}^*, x_{B_{u,n}^c}) dx_{u,n} - \int h(x_{u,n}) f_{X_{u,n}|Y_{B_{u,n}}}(x_{u,n} | y_{B_{u,n}}^*) dx_{u,n} \right| < \epsilon_{A1}.$$

Assumption A2. For the collection of neighborhoods in Assumption A1, with $B_{u,n}^+ = B_{u,n} \cup (u, n)$, there is a constant b , depending on ϵ_{A1} but not on U and N , such that

$$\sup_{u \in 1:U, n \in 1:N} |B_{u,n}^+| \leq b.$$

Assumption A3. There is a constant Q , independent of U and N , such that, for all u and n ,

$$Q^{-1} < f_{Y_{u,n}|X_{u,n}}(y_{u,n}^* | x_{u,n}) < Q$$

Assumption A4. There exists $\epsilon_{A4} > 0$, independent of U and N , such that the following holds. For each u, n , a set $C_{u,n} \subset (1:U) \times (0:N)$ exists such that $(\tilde{u}, \tilde{n}) \notin C_{u,n}$ implies $B_{u,n}^+ \cap B_{\tilde{u}, \tilde{n}}^+ = \emptyset$ and

$$\left| f_{X_{B_{\tilde{u}, \tilde{n}}^+}|X_{B_{u,n}^+}} - f_{X_{B_{\tilde{u}, \tilde{n}}^+}} \right| < \epsilon_{A4} f_{X_{B_{\tilde{u}, \tilde{n}}^+}}$$

Further, there is a uniform bound $|C_{u,n}| \leq c$.

The two mixing conditions in Assumptions A1 and A4 are subtly different. Assumption A1 describes a conditional mixing property dependent on the data, whereas A4 asserts a form of unconditional mixing. Although both capture a similar concept of weak coupling, conditional and unconditional mixing properties do not readily imply one another. Assumption A3 is a compactness condition of a type that has proved useful in the theory of particle filters despite the rarity of its holding exactly. Theorem 1 shows that these conditions let UBF compute the likelihood with a Monte Carlo variance of order $UN\mathcal{I}^{-1}$ with a bias of order $UN\epsilon$.

Theorem 1. Let ℓ^{MC} denote the Monte Carlo likelihood approximation constructed by UBF. Consider a limit with a growing number of bootstrap replicates, $\mathcal{I} \rightarrow \infty$, and suppose assumptions A1, A2 and A3. There are quantities $\epsilon(U, N)$ and $V(U, N)$, with bounds $|\epsilon| < \epsilon_{A1} Q^2$ and $V < Q^{4b} U^2 N^2$, such that

$$\mathcal{I}^{1/2}[\ell^{MC} - \ell - \epsilon UN] \xrightarrow[\mathcal{I} \rightarrow \infty]{d} \mathcal{N}[0, V], \quad (2)$$

where $\xrightarrow[\mathcal{I} \rightarrow \infty]{d}$ denotes convergence in distribution and $\mathcal{N}[\mu, \Sigma]$ is the normal distribution with mean μ and variance Σ . If additionally Assumption A4 holds, we obtain an improved variance bound

$$V < Q^{4b} UN(c + \epsilon_{A4}(UN - c)). \quad (3)$$

Proof. A complete proof is given in Sec. S3. Briefly, the assumptions imply a multivariate central limit theorem for $\{\ell_{u,n}^{MC}, (u, n) \in 1:U \times 1:N\}$ as $\mathcal{I} \rightarrow \infty$. The limiting variances and covariances are uniformly bounded, using Assumptions A2 and A3. Assumption A1 provides a uniform bound on the discrepancy between $\ell_{u,n}$ and mean of the Gaussian limit. This is enough to derive (2). Assumption A4 gives a stronger bound on covariances between sufficiently distant units, leading to (3). \square

Theorem 1 does not guarantee uniformity over U and N of the rate of convergence as $\mathcal{I} \rightarrow \infty$. However, it does guarantee that the polynomial bounds in (2) and (3) hold for sufficiently large \mathcal{I} . The COD is characterized by exponential bounds, and so Theorem 1 shows a specific sense in which UBF can avoid COD. Uniformity of the central limit convergence in Theorem 1 may be expected to hold via a Berry-Esseen theorem, but extension of existing Berry-Esseen results for dependent processes (Bentkus et al., 1997; Jirak, 2016) is beyond the scope of this article.

The approximation error for UBF can be divided into two sources: a localization bias due to conditioning on a finite neighborhood, and Monte Carlo error. The localization bias does not disappear in the limit as Monte Carlo effort increases. It does become small as the conditioning neighborhood increases, but the Monte Carlo effort grows exponentially in

the size of this neighborhood. Although the filtering inference is carried out using localization, the simulation of the process is carried out globally which avoids the introduction of additional boundary effects and ensures that the simulations comply with any constraints satisfied by the model for the latent process.

3 Adaptation and intermediate resampling

Theorem 1 shows that UBF can beat COD. However, UBF can perform poorly on long time series unless weak temporal dependence allows simulated sample paths to remain relevant over the course of a long time series. For example, we will find that UBF performs well on an epidemiological model (Sec. 5) but less well on a geophysical model (Sec. S8). It is sometimes necessary to select simulations consistent with the data, much as standard PF algorithms do. We look for approaches that build on the basic insight of UBF while having superior practical performance.

Whereas the full global filtering problem of drawing from $f_{\mathbf{X}_n|\mathbf{Y}_{1:n}}$ may be intractable via importance sampling methods, a version of this problem localized in space and time may nevertheless be feasible. The conditional density, $f_{\mathbf{X}_n|\mathbf{Y}_n, \mathbf{X}_{n-1}}$, is called the *adapted density*, and simulating from this density is called *adapted simulation*. For models where \mathbf{X}_{n-1} is highly informative about \mathbf{X}_n , importance sampling for adapted simulation may be much easier than the full filter calculation. The following adapted bagged filter (ABF) is constructed under a hypothesis that the adapted simulation problem is tractable, and it is applicable when the number of units is prohibitive for Monte Carlo sampling from the full filter distribution but not for sampling from the adapted distribution. In ABF, the adapted simulations are reweighted in a neighborhood of each unit and time point to construct a local approximation to the filtering problem which leads to an estimate of the likelihood. The pseudocode for ABF, below, reduces to UBF when using a single particle per replicate, $J = 1$.

ABF. Adapted bagged filter.

input: same as for UBF plus

particles per replicate, J

implicit loops:

u in $1:U$, n in $1:N$, i in $1:\mathcal{I}$, j in $1:J$

algorithm:

Initialize adapted simulation: $\mathbf{X}_{0,i}^A \sim f_{\mathbf{X}_0}(\mathbf{x}_0)$

For n in $1:N$

Proposals: $\mathbf{X}_{n,i,j}^P \sim f_{\mathbf{X}_n | \mathbf{X}_{1:U,n-1}}(\mathbf{x}_n | \mathbf{X}_{n-1,i}^A)$

Measurement weights: $w_{u,n,i,j}^M = f_{Y_{u,n} | X_{u,n}}(y_{u,n}^* | X_{u,n,i,j}^P)$

Adapted resampling weights: $w_{n,i,j}^A = \prod_{u=1}^U w_{u,n,i,j}^M$

Resampling: $\mathbb{P}[r(i) = a] = w_{n,i,a}^A \left(\sum_{k=1}^J w_{n,i,k}^A \right)^{-1}$

$\mathbf{X}_{n,i}^A = \mathbf{X}_{n,i,r(i)}^P$

$$w_{u,n,i,j}^P = \prod_{\tilde{n}=1}^{n-1} \left[\frac{1}{J} \sum_{k=1}^J \prod_{\tilde{u}: (\tilde{u}, \tilde{n}) \in B_{u,n}} w_{\tilde{u}, \tilde{n}, i, k}^M \right] \prod_{\tilde{u}: (\tilde{u}, n) \in B_{u,n}} w_{\tilde{u}, n, i, j}^M$$

End for

output:

$$\ell_{u,n}^{\text{MC}} = \log \left(\frac{\sum_{i=1}^{\mathcal{I}} \sum_{j=1}^J w_{u,n,i,j}^M w_{u,n,i,j}^P}{\sum_{i=1}^{\mathcal{I}} \sum_{j=1}^J w_{u,n,i,j}^P} \right)$$

ABF remedies a weakness of UBF by making each bootstrap filter adapted to the data. However, this benefit carries a cost, since adapted simulation is not immune from the curse of dimensionality. Therefore, we also consider an algorithm called ABF-IR which uses an intermediate resampling technique to carry out the adapted simulation. Intermediate resampling involves assessing the satisfactory progress of particles toward the subsequent observation at a collection of times between observations. This is well defined when the latent process has a continuous time representation, $\{\mathbf{X}(t)\}$, with observation times $t_{1:N}$. We write S intermediate resampling times as

$$t_{n-1} = t_{n,0} < t_{n,1} < \dots < t_{n,S} = t_n.$$

Carrying out an intermediate resampling procedure can have favorable scaling properties when S is proportional to U (Park and Ionides, 2020). In the case $S = 1$, ABF-IR reduces to ABF. Intermediate resampling was developed in the context of sequential Monte Carlo (Del Moral and Murray, 2015; Park and Ionides, 2020); however, the same theory and methodology can be applied to the simpler and easier problem of adapted simulation. ABF-IR employs a guide function to gauge the compatibility of each particle with future data. This is a generalization of the popular auxiliary particle filter (Pitt and Shepard, 1999). Only an ideal guide function fully addresses COD (Park and Ionides, 2020) and on nontrivial problems this is not available. However, practical guide functions can nevertheless improve performance.

The implementation in the ABF-IR pseudocode constructs the guide $g_{n,s,i,j}$ using a simulated moment method proposed by Park and Ionides (2020). The quantities $\mathbf{X}_{n,i,j}^G$, $V_{u,n,i}$, $\boldsymbol{\mu}_{n,s,i,j}^{\text{IP}}$, $V_{u,n,s,i,j}^{\text{meas}}$, $V_{u,n,s,i}^{\text{proc}}$ and $\theta_{u,n,s,i,j}$ constructed in ABF-IR are used only to construct $g_{n,s,i,j}$. Heuristically, we use guide simulations to approximate the variance of the increment in each particle between time points, and we augment the measurement variance to account for both dynamic variability and measurement error. The guide function affects numerical performance of the algorithm but not its correctness: it enables a computationally convenient approximation to improve performance on the intractable target problem. Our guide function supposes the availability of a deterministic function approximating evolution of the mean of the latent process, written as

$$\boldsymbol{\mu}(\mathbf{x}, s, t) \approx \mathbb{E}[\mathbf{X}(t) \mid \mathbf{X}(s) = \mathbf{x}].$$

Further, the guide requires that the measurement model has known conditional mean and variance as a function of the model parameter vector θ , written as

$$\begin{aligned} h_{u,n}(x_{u,n}) &= \mathbb{E}[Y_{u,n} \mid X_{u,n} = x_{u,n}] \\ \vec{v}_{u,n}(x_{u,n}, \theta) &= \text{Var}(Y_{u,n} \mid X_{u,n} = x_{u,n}; \theta) \end{aligned}$$

Also required for ABF-IR is an inverse function $\overleftarrow{v}_{u,n}$ such that

$$\vec{v}_{u,n}(x_{u,n}, \overleftarrow{v}_{u,n}(V, x_{u,n}, \theta)) = V.$$

ABF-IR. Adapted bagged filter with intermediate resampling.

input: same as for ABF plus

number of intermediate timesteps, S

measurement variance parameterizations, $\overleftarrow{v}_{u,n}$ and $\overrightarrow{v}_{u,n}$

approximate process and observation mean functions, $\boldsymbol{\mu}$ and $h_{u,n}$

implicit loops:

u in $1:U$, n in $1:N$, i in $1:\mathcal{I}$, j in $1:J$, j in $1:J$

algorithm:

Initialize adapted simulation: $\mathbf{X}_{0,i}^A \sim f_{\mathbf{X}_0}(\mathbf{x}_0)$

For n in $1:N$

Guide simulations: $\mathbf{X}_{n,i,j}^G \sim f_{\mathbf{X}_n|\mathbf{X}_{n-1}}(\mathbf{x}_n | \mathbf{X}_{n-1,i}^A)$

Guide sample variance: $V_{u,n,i} = \text{Var}\{h_{u,n}(X_{u,n,i,j}^G), j \text{ in } 1:J\}$

$g_{n,0,i,j}^R = 1$ and $\mathbf{X}_{n,0,i,j}^{\text{IR}} = \mathbf{X}_{n-1,i}^A$

For s in $1:S$

Intermediate proposals: $\mathbf{X}_{n,s,i,j}^{\text{IP}} \sim f_{\mathbf{X}_{n,s}|\mathbf{X}_{n,s-1}}(\cdot | \mathbf{X}_{n,s-1,i,j}^{\text{IR}})$

$\boldsymbol{\mu}_{n,s,i,j}^{\text{IP}} = \boldsymbol{\mu}(\mathbf{X}_{n,s,i,j}^{\text{IP}}, t_{n,s}, t_n)$

$V_{u,n,s,i,j}^{\text{meas}} = \overrightarrow{v}_u(\theta, \boldsymbol{\mu}_{u,n,s,i,j}^{\text{IP}})$

$V_{u,n,s,i}^{\text{proc}} = V_{u,n,i}(t_n - t_{n,s}) / (t_n - t_{n,0})$

$\theta_{u,n,s,i,j} = \overleftarrow{v}_u(V_{u,n,s,i,j}^{\text{meas}} + V_{u,n,s,i}^{\text{proc}}, \boldsymbol{\mu}_{u,n,s,i,j}^{\text{IP}})$

$g_{n,s,i,j} = \prod_{u=1}^U f_{Y_{u,n}|X_{u,n}}(y_{u,n}^* | \boldsymbol{\mu}_{u,n,s,i,j}^{\text{IP}}; \theta_{u,n,s,i,j})$

Guide weights: $w_{n,s,i,j}^G = g_{n,s,i,j} / g_{n,s-1,i,j}^R$

Resampling: $\mathbb{P}[r(i,j) = a] = w_{n,s,i,a}^G \left(\sum_{k=1}^J w_{n,s,i,k}^G \right)^{-1}$

$\mathbf{X}_{n,s,i,j}^{\text{IR}} = \mathbf{X}_{n,s,i,r(i,j)}^{\text{IP}}$ and $g_{n,s,i,j}^R = g_{n,s,i,r(i,j)}$

End For

Set $\mathbf{X}_{n,i}^A = \mathbf{X}_{n,S,i,1}^{\text{IR}}$

Measurement weights: $w_{u,n,i,j}^M = f_{Y_{u,n}|X_{u,n}}(y_{u,n}^* | X_{u,n,i,j}^G)$

$$w_{u,n,i,j}^P = \prod_{\tilde{n}=1}^{n-1} \left[\frac{1}{J} \sum_{a=1}^J \prod_{\tilde{u}:(\tilde{u},\tilde{n}) \in B_{u,n}} w_{\tilde{u},\tilde{n},i,a}^M \right] \prod_{\tilde{u}:(\tilde{u},n) \in B_{u,n}} w_{\tilde{u},n,i,j}^M$$

End for

output:

$$\ell_{u,n}^{\text{MC}} = \log \left(\frac{\sum_{i=1}^{\mathcal{I}} \sum_{j=1}^J w_{u,n,i,j}^M w_{u,n,i,j}^P}{\sum_{i=1}^{\mathcal{I}} \sum_{j=1}^J w_{u,n,i,j}^P} \right)$$

This guide function is applicable to spatiotemporal versions of a broad range of population and compartment models used to model dynamic systems in ecology, epidemiology, and elsewhere. Other guide functions could be developed and inserted into the ABF-IR algorithm, including other constructions considered by Park and Ionides (2020).

One might wonder why it is appropriate to keep many particle representations at intermediate timesteps while resampling down to a single representative at each observation time. An answer is that adaptive simulation can fail to track the observation sequence when one resamples down to a single particle too often (Sec. S2).

3.1 ABF-IR theory

We start by considering a deterministic limit for infinite Monte Carlo effort and explaining why the ABF and ABF-IR algorithms approximately target the likelihood function, subject to suitable mixing behavior. Subsequently, we consider the scaling properties as Monte Carlo effort increases. We adopt a convention that densities involving $Y_{u,n}$ are implicitly evaluated at the data, $y_{u,n}^*$, and densities involving $X_{u,n}$ are implicitly evaluated at $x_{u,n}$ unless otherwise specified. We write $A_{u,n}^+ = A_{u,n} \cup (u, n)$, matching the definition $B_{u,n}^+ = B_{u,n} \cup (u, n)$. The essential ingredient in all the algorithms is a localization of the likelihood, which may be factorized sequentially as

$$f_{Y_{1:U}, 1:N} = \prod_{n=1}^N \prod_{u=1}^U f_{Y_{u,n} | Y_{A_{u,n}}} = \prod_{n=1}^N \prod_{u=1}^U \frac{f_{Y_{A_{u,n}^+}}}{f_{Y_{A_{u,n}}}}.$$

In particular, the approximations assume that the full history $A_{u,n}$ can be well approximated by a neighborhood $B_{u,n} \subset A_{u,n}$. UBF approximates $f_{Y_{u,n} | Y_{A_{u,n}}}$ by

$$f_{Y_{u,n} | Y_{B_{u,n}}} = \frac{f_{Y_{B_{u,n}^+}}}{f_{Y_{B_{u,n}}}} = \frac{\int f_{Y_{B_{u,n}^+} | X_{B_{u,n}^+}} f_{X_{B_{u,n}^+}} dx_{B_{u,n}^+}}{\int f_{Y_{B_{u,n}} | X_{B_{u,n}}} f_{X_{B_{u,n}}} dx_{B_{u,n}}}.$$

For $B \subset 1:U \times 1:N$, define $B^{[m]} = B \cap (1:U \times \{m\})$. ABF and ABF-IR build on the following identity,

$$f_{Y_{A_{u,n}}} = \int f_{\mathbf{X}_0} \left[\prod_{m=1}^n f_{\mathbf{X}_m | \mathbf{X}_{m-1}, \mathbf{Y}_m} f_{Y_{A_{u,n}^{[m]} | \mathbf{X}_{m-1}}} \right] d\mathbf{x}_{0:n},$$

where $f_{\mathbf{X}_m|\mathbf{X}_{m-1},\mathbf{Y}_m}$ is called the adapted transition density. The adapted process (i.e., a stochastic process following the adapted transition density) can be interpreted as a one-step greedy procedure using the data to guide the latent process. Let $g_{\mathbf{X}_{0:N},\mathbf{X}_{1:N}^P}(\mathbf{x}_{0:N},\mathbf{x}_{1:N}^P)$ be the joint density of the adapted process and the proposal process,

$$g_{\mathbf{X}_{0:N},\mathbf{X}_{1:N}^P}(\mathbf{x}_{0:N},\mathbf{x}_{1:N}^P) = f_{\mathbf{X}_0}(\mathbf{x}_0) \times \prod_{n=1}^N f_{\mathbf{X}_n|\mathbf{X}_{n-1},\mathbf{Y}_n}(\mathbf{x}_n|\mathbf{x}_{n-1},\mathbf{y}_n^*) f_{\mathbf{X}_n|\mathbf{X}_{n-1}}(\mathbf{x}_n^P|\mathbf{x}_{n-1}). \quad (4)$$

Using the convention that an empty density f_{Y_\emptyset} evaluates to 1, we define

$$\gamma_B = \prod_{m=1}^N f_{Y_{B[m]}|\mathbf{X}_{m-1}}(y_{B[m]}^*|\mathbf{X}_{m-1}).$$

Denoting \mathbb{E}_g for expectation for $(\mathbf{X}_{0:N},\mathbf{X}_{1:N}^P)$ having density $g_{\mathbf{X}_{0:N},\mathbf{X}_{1:N}^P}$, we have $f_{Y_{A_{u,n}}} = \mathbb{E}_g[\gamma_{A_{u,n}}]$ and thus

$$f_{Y_{u,n}|Y_{A_{u,n}}} = \frac{\mathbb{E}_g[\gamma_{A_{u,n}^+}]}{\mathbb{E}_g[\gamma_{A_{u,n}}]}.$$

Estimating this ratio by Monte Carlo sampling from g is problematic due to the growing size of $A_{u,n}$. Thus, ABF and ABF-IR make a localized approximation,

$$\frac{\mathbb{E}_g[\gamma_{A_{u,n}^+}]}{\mathbb{E}_g[\gamma_{A_{u,n}}]} \approx \frac{\mathbb{E}_g[\gamma_{B_{u,n}^+}]}{\mathbb{E}_g[\gamma_{B_{u,n}}]}. \quad (5)$$

The conditional log likelihood estimate $\ell_{u,n}^{\text{MC}}$ in ABF and ABF-IR come from replacing the expectations on the right hand side of (5) with averages over Monte Carlo replicates of simulations from the adapted process. To see that we expect the approximation in (5) to hold when dependence decays across spatiotemporal distance, we can write

$$\begin{aligned} \gamma_{A_{u,n}} &= \gamma_{B_{u,n}} \gamma_{B_{u,n}^c} \\ \gamma_{A_{u,n}^+} &= \gamma_{B_{u,n}^+} \gamma_{B_{u,n}^c}, \end{aligned}$$

where $B_{u,n}^c$ is the complement of $B_{u,n}$ in $A_{u,n}$. Under our assumptions, the term corresponding to $\gamma_{B_{u,n}^c}$ approximately cancels in the numerator and denominator of the right hand side of (5).

Since ABF is ABF-IR with $S = 1$, we focus attention on ABF-IR. At a conceptual level, the localized likelihood estimate in ABF-IR has the same structure as its UBF counterpart. However, ABF-IR additionally requires the capability to satisfactorily implement adapted simulation. Adapted simulation is a local calculation, making it an easier task than the global operation of filtering. Nevertheless, adapted simulation via importance sampling is vulnerable to COD for sufficiently large values of U . For a continuous time model, the use of $S > 1$ is motivated by a result that guided intermediate resampling can reduce, or even remove, the COD in the context of a particle filtering algorithm (Park and Ionides, 2020). Assumptions B1–B4 below are analogous to A1–A4 and are non-asymptotic assumptions involving $\epsilon_{B1} > 0$, $\epsilon_{B4} > 0$ and $Q > 1$ which are required to hold uniformly over space and time. Assumptions B5–B7 control the Monte Carlo error arising from adapted simulation. B5 is a stability property which asserts that the effect of the latent process on the future of the adapted process decays over time. Assumption B6 is a non-asymptotic bound on Monte Carlo error for a single step of adapted simulation. The scaling of the constant \mathcal{C}_0 with U , N and S in Assumption B6 has been studied by Park and Ionides (2020), where it was established that setting $S = U$ can lead to \mathcal{C}_0 being constant, when using an ideal guide function, or slowly growing with U otherwise. The ϵ_{B6}^{-3} error rate in Assumption B6 follows from balancing the two sources of error defined in the statement of Theorem 2 of Park and Ionides (2020). Assumption B7 can be guaranteed by the construction of the algorithm, if independently generated Monte Carlo random variables are used for building the guide function and the one-step prediction particles. The asymptotic limit in Theorem 2 arises as the number of replicates increases.

Assumption B1. *There is an $\epsilon_{B1} > 0$, independent of U and N , and a collection of neighborhoods $\{B_{u,n} \subset A_{u,n}, u \in 1:U, n \in 1:N\}$ such that the following holds for all u and n , and any bounded real-valued function $|h(x)| \leq 1$. Setting $A = A_{u,n}$, $B = B_{u,n}$, $f_A(x_A) = f_{Y_A|X_A}(y_A^*|x_A)$, and $f_B(x_B) = f_{Y_B|X_B}(y_B^*|x_B)$, so that we have the identity*

$$f_{X_{u,n}|Y_A}(x|y_A^*) = \frac{\mathbb{E}_g[f_A(X_A^P) f_{X_{u,n}|X_{A[n]}, \mathbf{X}_{n-1}}(x|X_{A[n]}^P, \mathbf{X}_{n-1})]}{\mathbb{E}_g[f_A(X_A^P)]},$$

we require that

$$\left| \int h(x) \left\{ \frac{\mathbb{E}_g[f_A(X_A^P) f_{X_{u,n}|X_{A^{[n]}}, \mathbf{X}_{n-1}}(x|X_{A^{[n]}}, \mathbf{X}_{n-1})]}{\mathbb{E}_g[f_A(X_A^P)]} - \frac{\mathbb{E}_g[f_B(X_B^P) f_{X_{u,n}|X_{B^{[n]}}, \mathbf{X}_{n-1}}(x|X_{B^{[n]}}, \mathbf{X}_{n-1})]}{\mathbb{E}_g[f_B(X_B^P)]} \right\} dx \right| < \epsilon_{B1}.$$

Assumption B2. The bound $\sup_{u \in 1:U, n \in 1:N} |B_{u,n}^+| \leq b$ in Assumption A2 applies for the neighborhoods defined in Assumption B1. This also implies there is a finite maximum temporal depth for the collection of neighborhoods, defined as

$$d_{\max} = \sup_{(u,n)} \sup_{(\tilde{u}, \tilde{n}) \in B_{u,n}} |n - \tilde{n}|.$$

Assumption B3. Identically to Assumption A3, $Q^{-1} < f_{Y_{u,n}|X_{u,n}}(y_{u,n}^* | x_{u,n}) < Q$.

Assumption B4. We use subscripts of g to denote marginal and conditional densities derived from (4). Suppose there is an ϵ_{B4} , independent of U and N , such that the following holds. For each u and n , a set $C_{u,n} \subset (1:U) \times (0:N)$ exists such that $(\tilde{u}, \tilde{n}) \notin C_{u,n}$ implies $B_{u,n}^+ \cap B_{\tilde{u}, \tilde{n}}^+ = \emptyset$ and

$$\begin{aligned} |g_{X_{B_{\tilde{u}, \tilde{n}} \cup B_{u,n}}^P} - g_{X_{B_{\tilde{u}, \tilde{n}}}^P} g_{X_{B_{u,n}}^P}| &< (1/2) \epsilon_{B4} g_{X_{B_{\tilde{u}, \tilde{n}} \cup B_{u,n}}^P} \\ |g_{X_{B_{\tilde{u}, \tilde{n}}}^P | \mathbf{X}_{0:N}} g_{X_{B_{u,n}}^P | \mathbf{X}_{0:N}} - g_{X_{B_{\tilde{u}, \tilde{n}} \cup B_{u,n}}^P | \mathbf{X}_{0:N}}| &< (1/2) \epsilon_{B4} g_{X_{B_{\tilde{u}, \tilde{n}} \cup B_{u,n}}^P | \mathbf{X}_{0:N}} \end{aligned}$$

Further, there is a uniform bound $|C_{u,n}| \leq c$.

Assumption B5. There is a constant K , independent of U and N , such that, for any $0 \leq d \leq d_{\max}$, any $n \geq K + d$, and any set $D \subset (1:U) \times (n:n-d)$,

$$\begin{aligned} |g_{X_D | \mathbf{X}_{n-d-K}}(x_D | \mathbf{x}_{n-d-K}^{(1)}) - g_{X_D | \mathbf{X}_{n-d-K}}(x_D | \mathbf{x}_{n-d-K}^{(2)})| \\ < \epsilon_{B5} g_{X_D | \mathbf{X}_{n-d-K}}(x_D | \mathbf{x}_{n-d-K}^{(1)}) \end{aligned}$$

holds for all $\mathbf{x}_{n-d-K}^{(1)}$, $\mathbf{x}_{n-d-K}^{(2)}$, and x_D .

Assumption B6. Let h be a bounded function with $|h(x)| \leq 1$. Let $\mathbf{X}_{n,S,j,i}^{\text{IR}}$ be the Monte Carlo quantity constructed in ABF-IR, conditional on $\mathbf{X}_{n-1,S,i}^{\text{A}} = \mathbf{x}_{n-1,S,i}^{\text{A}}$. There is a constant $\mathcal{C}_0(U, N, S)$ such that, for all $\epsilon_{\text{B6}} > 0$ and $\mathbf{x}_{n-1,S,i}^{\text{A}}$, whenever the number of particles satisfies $J > \mathcal{C}_0(U, N, S)/\epsilon_{\text{B6}}^3$,

$$\left| \mathbb{E} \left[\frac{1}{J} \sum_{j=1}^J h(\mathbf{X}_{n,S,j,i}^{\text{IR}}) \right] - \mathbb{E}_g[h(\mathbf{X}_n) \mid \mathbf{X}_{n-1} = \mathbf{x}_{n-1,S,i}^{\text{A}}] \right| < \epsilon_{\text{B6}}.$$

Assumption B7. For $1 \leq n \leq N$, the Monte Carlo random variable $X_{n,i}^{\text{A}}$ is independent of $w_{u,n,i,j}^{\text{M}}$ conditional on $X_{n-1,i}^{\text{A}}$.

Theorem 2. Let ℓ^{MC} denote the Monte Carlo likelihood approximation constructed by ABF-IR, or by ABF since this is the special case of ABF-IR with $S = 1$. Consider a limit with a growing number of bootstrap replicates, $\mathcal{I} \rightarrow \infty$, and suppose assumptions B1, B2, B3, B5, B6 and B7. Suppose the number of particles J exceeds the requirement for B6. There are quantities $\epsilon(U, N)$ and $V(U, N)$ with $|\epsilon| < Q^2\epsilon_{\text{B1}} + 2Q^{2b}(\epsilon_{\text{B5}} + (K + d_{\text{max}})\epsilon_{\text{B6}})$ and $V < Q^{4b}U^2N^2$ such that

$$\mathcal{I}^{1/2}[\ell^{\text{MC}} - \ell - \epsilon UN] \xrightarrow[\mathcal{I} \rightarrow \infty]{d} \mathcal{N}[0, V].$$

If additionally Assumption B4 holds, we obtain an improved rate of

$$V < Q^{4b}NU \{c + (\epsilon_{\text{B4}} + 3\epsilon_{\text{B5}} + 4(K + d_{\text{max}})\epsilon_{\text{B6}})(NU - c)\}$$

Proof. A full proof is provided in Sec. S4. The extra work to prove Theorem 2 beyond the argument for Theorem 1 is to bound the error arising from the importance sampling approximation to a draw from the adapted transition density. This bound is constructed using Assumptions B5, B6 and B7. The remainder of the proof follows the same approach as Theorem 1, with the adapted process replacing the unconditional latent process. \square

The theoretical results foreshadow our empirical observations (Sec. 4) that the relative performance of UBF, ABF and ABF-IR is situation-dependent. Assumption A4 is a mixing assumption for the unconditional latent process, whereas Assumption B4 replaces this with

a mixing assumption for the adapted process conditional on the data. For a non-stationary process, Assumption A4 may fail to hold uniformly in U whereas the adapted process may provide stable tracking of the latent process (Sec. S2). When Assumption A4 holds, UBF can benefit from not requiring Assumptions B5, B6 and B7. Adapted simulation is an easier problem than filtering, but nevertheless can become difficult in high dimensions, with the consequence that Assumption B6 could require large \mathcal{C}_0 . The tradeoff between ABF and ABF-IR depends on the effectiveness of the guide function for the problem at hand. Intermediate resampling and guide function calculation require additional computational resources, which will necessitate smaller values of \mathcal{I} and J . In some situations, the improved scaling properties of ABF-IR compared to ABF, corresponding to a lower value of \mathcal{C}_0 , will outweigh this cost.

4 Examples

We compare the performance of the three bagged filters (UBF, ABF and ABF-IR) against each other and against alternative plug-and-play approaches. The plug-and-play property facilitates numerical implementation for general classes of models, and all the algorithms and models under consideration are implemented in the `spatPomp` R package (Asfaw et al., 2021b). Ensemble Kalman filter (EnKF) methods propagate the ensemble members by simulation from the dynamic model and then update the ensemble to assimilate observations using a Gaussian-inspired rule (Evensen and van Leeuwen, 1996; Lei et al., 2010). The block particle filter (BPF, Rebeschini and van Handel, 2015; Ng et al., 2002) partitions the latent space and combines independently drawn components from each partition. BPF overcomes COD under weak coupling assumptions (Rebeschini and van Handel, 2015). Unlike these two methods, our bagged filters modify particles only according to the latent dynamics. Thus, our methods respect conservation laws and continuity or smoothness conditions obeyed by the dynamic model. We also compare with a guided intermediate resampling filter (GIRF, Park and Ionides, 2019), one of many variants of the particle filter designed to scale to larger

numbers of units than are possible with a basic particle filter.

First, in Sec. 4.1, we consider a spatiotemporal Gaussian process for which the exact likelihood is available via a Kalman filter. We see in Fig. 1 that ABF-IR can have a considerable advantages over UBF and ABF for problems with an intermediate level of coupling. Then, in Sec. 4.2, we develop a model for measles transmission within and between cities. The measles model is weakly coupled, leading to successful performance for all three bagged filters. This class of metapopulation models was the primary motivation for the development of these methodologies. In Sec. 4.3 we demonstrate an extension from likelihood evaluation to likelihood maximization for the measles model. Additionally, in Sec. S8, we compare performance on the Lorenz-96 model, a highly coupled system used to test inference methods for geophysical applications.

4.1 Correlated Brownian motion

Suppose $\mathbf{X}(t) = \Omega \mathbf{W}(t)$ where $\mathbf{W}(t) = W_{1:U}(t)$ comprises U independent standard Brownian motions, and $\Omega_{u,\tilde{u}} = \rho^{d(u,\tilde{u})}$ with $d(u, \tilde{u})$ being the circle distance,

$$d(u, \tilde{u}) = \min(|u - \tilde{u}|, |u - \tilde{u} + U|, |u - \tilde{u} - U|).$$

Set $t_n = n$ for $n = 0, 1, \dots, N$ with initial value $\mathbf{X}(0) = \mathbf{0}$ and suppose measurement errors are independent and normally distributed, $Y_{u,n} = X_{u,n} + \eta_{u,n}$ with $\eta_{u,n} \sim \mathcal{N}(0, \tau^2)$. The parameter ρ determines the strength of the spatial coupling.

Fig. 1 shows how the bagged filters scale on this Gaussian model, compared to a standard particle filter (PF), a guided intermediate resampling filter (GIRF), a block particle filter (BPF), and an ensemble Kalman filter. For our numerical results, we use $\tau = 1$, $\rho = 0.4$ and $N = 50$. The algorithmic parameters and run times are listed in Sec. S5, together with a plot of the simulated data and supplementary discussion. In this case, the exact likelihood is computable via the Kalman filter (KF). Since EnKF is based on a Gaussian approximation, it is also exact in this case, up to a small Monte Carlo error. The GIRF framework encompasses lookahead particle filter techniques, such as the auxiliary particle

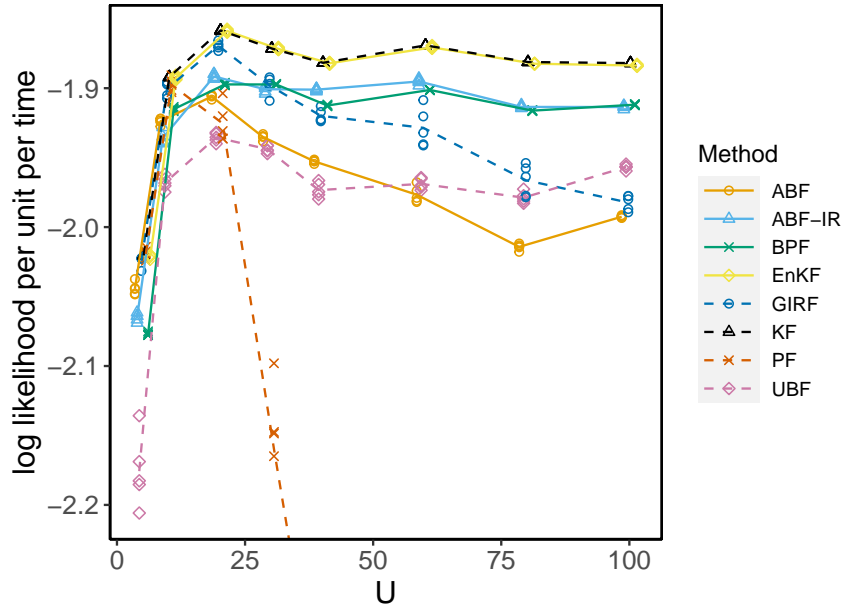


Figure 1: log likelihood estimates for a correlated Brownian motion model of various dimensions. UBF, ABF and ABF-IR are compared with a guided intermediate resampling filter (GIRF), standard particle filter (PF), block particle filter (BPF) and ensemble Kalman filter (EnKF). The exact likelihood was computed via a Kalman filter (KF).

filter (Pitt and Shepard, 1999), and intermediate resampling techniques (Del Moral et al., 2017). GIRF methods combining these techniques were found to perform better than either of these component techniques alone (Park and Ionides, 2020). Thus, GIRF here represents a state-of-the-art auxiliary particle filter that targets the complete joint filter density for all units. We use the general-purpose, plug-and-play implementation of GIRF provided by the `spatPomp` R package (Asfaw et al., 2021a); for a Gaussian model, one can calculate an ideal guide function for GIRF but that was not used. PF works well for small values of U in Fig. 1 and rapidly starts struggling as U increases. GIRF behaves comparably to PF for small U but its performance is maintained for larger U . ABF and ABF-IR have some efficiency loss, for small U , relative to PF and GIRF due to the localization involved in the filter weighting, but for large U this cost is paid back by the benefit of the reduced Monte Carlo variability. UBF has a larger efficiency loss for small U , but its favorable scaling properties lead it to overtake ABF for larger U . BPF shows stable scaling and modest efficiency loss. This linear Gaussian SpatPOMP model provides a simple scenario to demonstrate scaling behavior. For filters that cannot take direct advantage of the Gaussian property of the model, we see that there is a tradeoff between efficiency at low U and scalability. This is unavoidable, since there is no known algorithm that is simultaneously fully efficient (up to Monte Carlo error), scalable, and applicable to general SpatPOMP models. We now explore this tradeoff empirically on to a more complex SpatPOMP exemplifying the nonlinear non-Gaussian models motivating our new filtering approach.

4.2 Spatiotemporal measles epidemics

Data analysis for spatiotemporal systems featuring nonlinear, nonstationary mechanisms and partial observability has been a longstanding open challenge for ecological and epidemiological analysis (Bjørnstad and Grenfell, 2001). A compartment modeling framework for spatiotemporal population dynamics divides the population at each spatial location into categories, called compartments, which are modeled as homogeneous. Spatiotemporal compartment models can be called patch models or metapopulation models in an ecological

context. Ensemble Kalman filter (EnKF) methods provide a state-of-the-art approach to inference for metapopulation models (Li et al., 2020) despite concerns that the approximations inherent in the EnKF can be problematic for models that are highly nonlinear or non-Gaussian (Ades and Van Leeuwen, 2015). Our bagged filter methodologies have theoretical guarantees for arbitrarily nonlinear and non-Gaussian models, while having improved scaling properties compared to particle filters.

We consider a spatiotemporal model for disease transmission dynamics of measles within and between multiple cities, based on the model of Park and Ionides (2020) which adds spatial interaction to the compartment model presented by He et al. (2010). The model compartmentalizes the population of each city into susceptible (S), exposed (E), infectious (I), and recovered/removed (R) categories. The number of individuals in each compartment city u at time t are denoted by integer-valued random variables $S_u(t)$, $E_u(t)$, $I_u(t)$, and $R_u(t)$. The population dynamics are written in terms of counting processes $N_{\bullet\bullet,u}(t)$ enumerating cumulative transitions in city u , up to time t , between compartments identified by the subscripts. We model the U largest cities in the UK, ordered in decreasing size so that $u = 1$ corresponds to London. We vary U to test methodologies on a hierarchy of filtering challenges. Our model is described by the following system of stochastic differential equations, for $u = 1, \dots, U$,

$$\begin{aligned} dS_u(t) &= dN_{BS,u}(t) - dN_{SE,u}(t) - dN_{SD,u}(t) \\ dE_u(t) &= dN_{SE,u}(t) - dN_{EI,u}(t) - dN_{ED,u}(t) \\ dI_u(t) &= dN_{EI,u}(t) - dN_{IR,u}(t) - dN_{ID,u}(t) \end{aligned}$$

Here, $N_{BS,u}(t)$ models recruitment into the susceptible population, and $N_{\bullet D,u}(t)$ models emigration and death. The total population $P_u(t) = S_u(t) + E_u(t) + I_u(t) + R_u(t)$ is calculated by smoothing census data and is treated as known. The number of recovered individuals $R_u(t)$ in city u is therefore defined implicitly. $N_{SE,u}(t)$ is modeled as negative binomial death processes (Bretó et al., 2009; Bretó and Ionides, 2011) with over-dispersion parameter σ_{SE} ,

and rate given by

$$\begin{aligned} \mathbb{E}[N_{SE,u}(t+dt) - N_{SE,u}(t)] &= \beta(t) S_u(t) \left[\left(\frac{I_u + \iota}{P_u} \right)^\alpha \right. \\ &\quad \left. + \sum_{\tilde{u} \neq u} \frac{v_{u\tilde{u}}}{P_u} \left\{ \left(\frac{I_{\tilde{u}}}{P_{\tilde{u}}} \right)^\alpha - \left(\frac{I_u}{P_u} \right)^\alpha \right\} \right] dt + o(dt), \end{aligned} \quad (6)$$

where $\beta(t)$ models seasonality driven by high contact rates between children at school, described by

$$\beta(t) = \begin{cases} (1 + a(1-p)p^{-1}) \bar{\beta} & \text{during school term,} \\ (1-a) \bar{\beta} & \text{during vacation} \end{cases}$$

with $p = 0.759$ being the proportion of the year taken up by the school terms, $\bar{\beta}$ is the mean transmission rate, and a measures the reduction of transmission during school holidays. In (6), α is a mixing exponent modeling inhomogeneous contact rates within a city, and ι models immigration of infected individuals which is appropriate when analyzing a subset of cities that cannot be treated as a closed system. The number of travelers from city u to \tilde{u} is denoted by $v_{u\tilde{u}}$. Here, $v_{u\tilde{u}}$ is constructed using the gravity model of Xia et al. (2004),

$$v_{u\tilde{u}} = G \cdot \frac{\bar{d}}{\bar{P}^2} \cdot \frac{P_u \cdot P_{\tilde{u}}}{d(u, \tilde{u})},$$

where $d(u, \tilde{u})$ denotes the distance between city u and city \tilde{u} , P_u is the average population for city u across time, \bar{P} is the average population across cities, and \bar{d} is the average distance between a randomly chosen pair of cities. Here, we model $v_{u\tilde{u}}$ as fixed through time and symmetric between any two arbitrary cities, though a natural extension would allow for temporal variation and asymmetric movement between two cities. The transition processes $N_{EI,u}(t)$, $N_{IR,u}(t)$ and $N_{\bullet D,u}(t)$ are modeled as conditional Poisson processes with per-capita rates μ_{EI} , μ_{IR} and $\mu_{\bullet D}$ respectively, and we fix $\mu_{\bullet D} = 50 \text{ year}^{-1}$. The birth process $N_{BS,u}(t)$ is an inhomogeneous Poisson processes with rate $\mu_{BS,u}(t)$, given by interpolated census data.

To complete the model specification, we must describe the measurement process. Let $Z_{u,n} = N_{IR,u}(t_n) - N_{IR,u}(t_{n-1})$ be the number of removed infected individuals in the n th reporting interval. Suppose that cases are quarantined once they are identified, so that

reported cases comprise a fraction ρ of these removal events. The case report $y_{u,n}^*$ is modeled as a realization of a discretized conditionally Gaussian random variable $Y_{u,n}$, defined for $y > 0$ via

$$\begin{aligned} \mathbb{P}[Y_{u,n}=y \mid Z_{u,n}=z] &= \Phi(y + 0.5; \rho z, \rho(1 - \rho)z + \psi^2 \rho^2 z^2) \\ &\quad - \Phi(y - 0.5; \rho z, \rho(1 - \rho)z + \psi^2 \rho^2 z^2) \end{aligned} \quad (7)$$

where $\Phi(\cdot; \mu, \sigma^2)$ is the $\mathcal{N}(\mu, \sigma^2)$ cumulative distribution function, and ψ models overdispersion relative to the binomial distribution. For $y = 0$, we replace $y - 0.5$ by $-\infty$ in (7).

This model includes many features that have been proposed to be relevant for understanding measles transmission dynamics (He et al., 2010). Our plug-and-play methodology permits consideration of all these features, and readily extends to the investigation of further variations. Likelihood-based inference via plug-and-play methodology therefore provides a framework for evaluating which features of a dynamical model are critical for explaining the data (King et al., 2008). By contrast, Xia et al. (2004) developed a linearization for a specific spatiotemporal measles model which is numerically convenient but not readily adaptable to assess alternative model choices. Fig. 2 shows a simulation from our model, showing that trajectories from this model can capture some features of the system that have been hard to understand: how can it be that disease transmission dynamics between locations have important levels of interaction yet are not locked in synchrony (Becker et al., 2020)? Here, we are testing statistical tools rather than engaging directly in the scientific debate so we test methods on the simulated data.

We first assess the scaling properties of the filters on the measles model by evaluating the likelihood over varying numbers of units, U , for fixed parameters. The results are given in Fig. 3, with additional information about timing, algorithmic choices, parameter values and a plot of the data provided in Sec. S6. In Fig. 3, the log likelihood per unit per time increases with U because city size decreases with U . Smaller cities have fewer measles cases, resulting in a narrower and taller probability density function. Fig. 3 shows a rapid decline in the performance of the particle filter (PF) beyond $U = 4$. This is a challenging

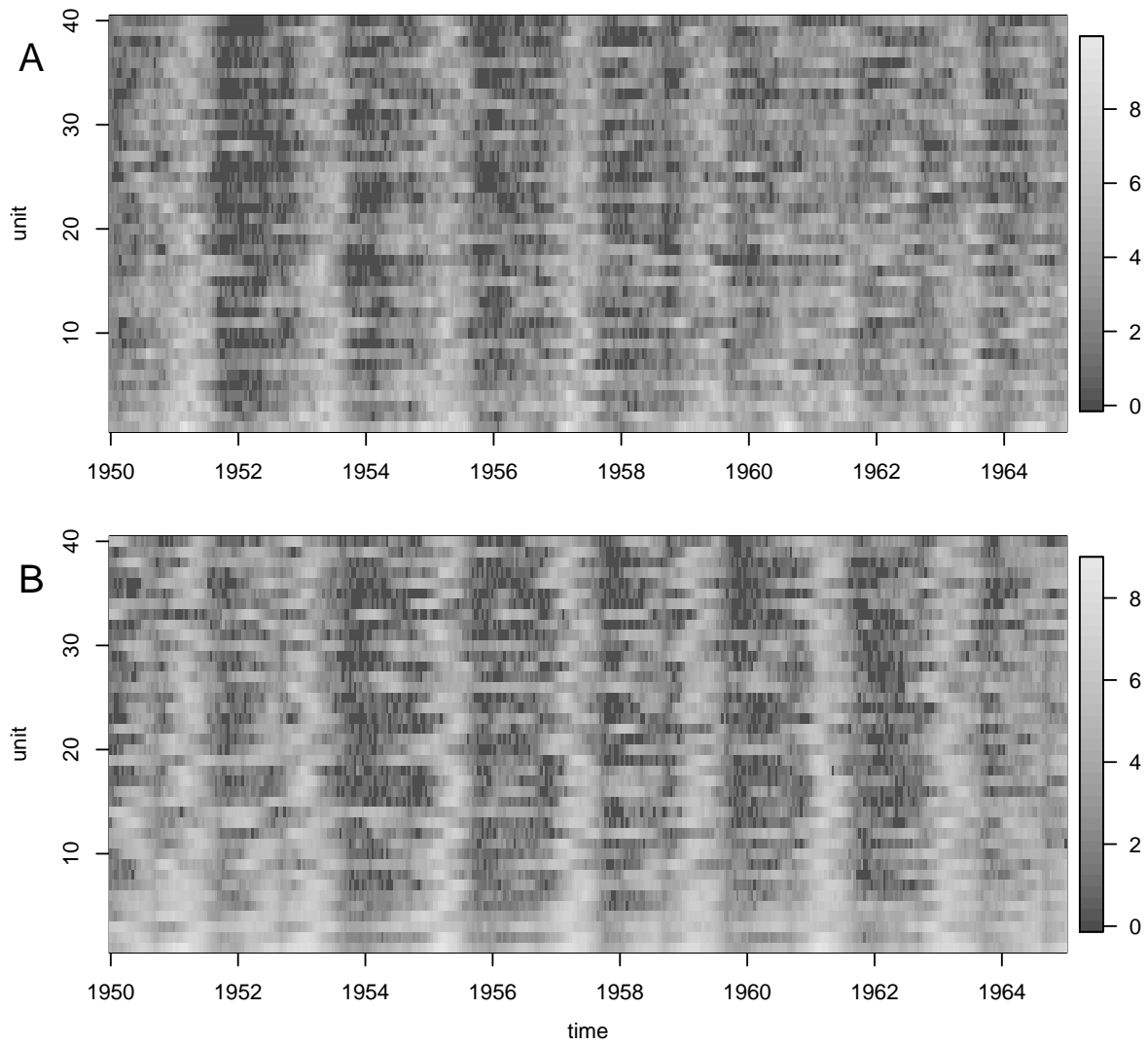


Figure 2: $\text{Log}(\text{reported cases} + 1)$ for (A) the measles simulation used for the likelihood slice; (B) the corresponding UK measles data. The simulation shares the biennial pattern, with most but not all cities locked in phase most of the time.

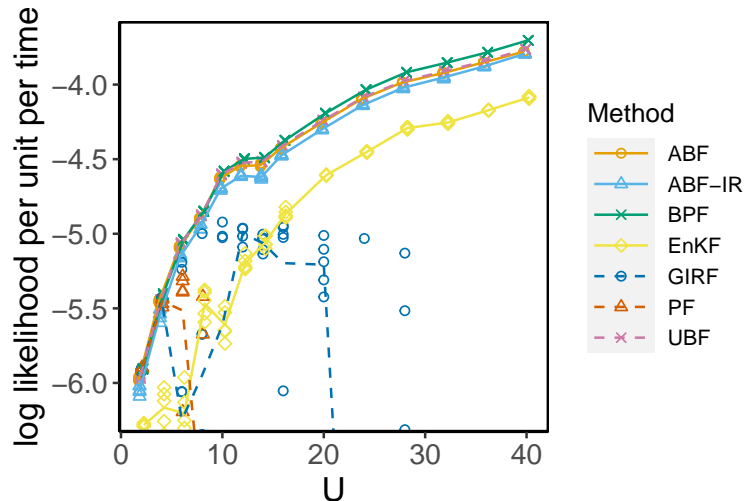


Figure 3: log likelihood estimates for simulated data from the measles model of various dimensions. UBF, ABF and ABF-IR are compared with a guided intermediate resampling filter (GIRF), a standard particle filter (PF), a block particle filter (BPF) and an ensemble Kalman filter (EnKF).

filtering problem, with dynamics including local fadeouts and high stochasticity in each city stabilized at the metapopulation level by the coupling. In this example, GIRF performs poorly suggesting that the simulated moment guide function is less than successful. We used the general-purpose implementation of GIRF in the `spatPomp` package, and there might be room for improvement by developing a model-specific guide function. ABF-IR uses the same guide function, and this may explain why ABF-IR performs worse than ABF here, though ABF-IR is much less sensitive than GIRF to the quality of the guide. ABF and UBF are competing with BPF as winners on this challenge. The bagged filters and BPF have substantial advantages compared to EnKF, amounting to more than 0.2 log likelihood units per observation. We suspect that the limitations of EnKF on this problem are due to the nonlinearity, non-Gaussianity, and discreteness of fadeout and reintroduction dynamics. All the algorithms have various tuning parameters that could influence the results. Some investigations of alternatives are presented in Secs. S6, S7 and S12. Generalizable conclusions are hard to infer from numerical comparisons of complex algorithms on complex models.

Experimentation with different methods, and their tuning parameters, is recommended when investigating a new model.

Fig. 4(A) demonstrates an application of ABF to the task of computing a slice of the likelihood function over the coupling parameter, G , for simulated data. This slice varies G while fixing the other parameters at the values used for the simulation. Fig. 4(B) shows a similar plot calculated using BPF with comparable computational effort. Both ABF and BPF are successful here, though BPF is more computationally efficient. By contrast, Fig. 4(C) shows that EnKF has substantial bias in estimating G , as well as considerably lower likelihood. Likelihood slices have less inferential value than likelihood profiles, but provide a computationally and conceptually simpler setting that can be insightful. Scientifically, the slices in Fig. 4 give an upper bound on the identifiability of G from such data, since the likelihood slice provides statistically efficient inference when all other parameters are known.

4.3 Likelihood maximization and profile likelihood

Likelihood evaluation via filtering does not by itself enable parameter estimation for POMP models, however it provides a foundation for Bayesian and likelihood-based inference. In particular, filtering algorithms can be modified to carry out likelihood maximization by stochastically perturbing parameters in a sequence of filtering operations with decreasing perturbation variance (Ionides et al., 2015). We demonstrate this for the measles model in Fig. 5 using an iterated bagged filter algorithm which is fully described in Sec. S11.

Monte Carlo methods for computing and maximizing the log likelihood suffer from bias and variance, both of which can be considerable for large datasets and complex models. Appropriate inference methodology, such as Monte Carlo adjusted profile (MCAP) confidence intervals, can accommodate substantial Monte Carlo variance so long as the bias is slowly varying across the statistically plausible region of the parameter space (Ionides et al., 2017; Ning et al., 2021). Fig. 5 constructs an MCAP 95% confidence interval for the coupling parameter, G , using an iterated unadapted bagged filter to maximize over the parameters, a , $\bar{\beta}$, σ_{SE} , ψ , μ_{EI} and μ_{IR} . This simulation study, carried out with $U = 20$ and $N = 208$,

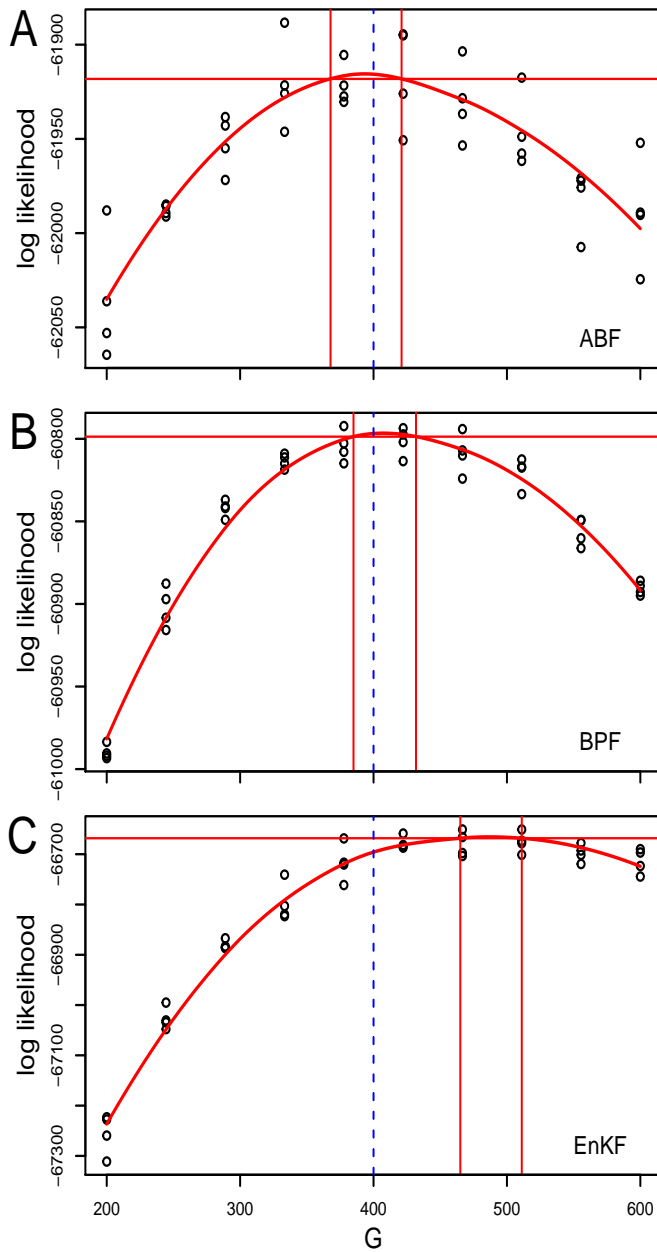


Figure 4: Likelihood slices varying the coupling parameter, for the measles model with $U = 40$ cities, computed via (A) ABF; (B) BPF; (C) EnKF. The solid perpendicular lines construct 95% Monte Carlo adjusted confidence intervals (Ionides et al., 2017). The true parameter value is identified by a blue dashed line.

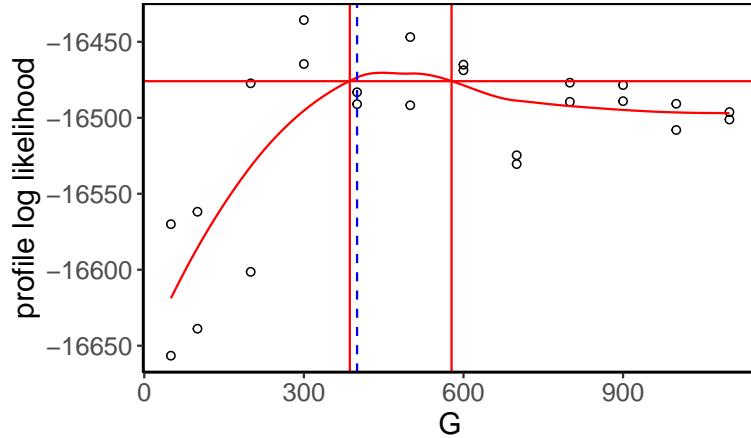


Figure 5: An iterated bagged filter used to maximize the likelihood, compute a profile likelihood, and hence construct a confidence interval. The profiling is carried out over the coupling parameter, G .

shows that G is identifiable via likelihood-based inference in the absence of assumptions about these parameters.

5 Discussion

The pseudocode presented for the bagged filters describes how the outputs are calculated given the inputs, but does not prescribe details of how these quantities are calculated. There is scope for implementations to trade off memory, computation and communication by varying decisions on how the loops defined in the pseudocode are coded, including decisions on memory over-writing and parallelization. This article focuses on the logical structure of the algorithms, leaving room for future research on implementation-specific considerations, though some supplementary discussion of memory-efficient implementation is given in Sec. S9.

Plug-and-play inference based on sequential Monte Carlo likelihood evaluation has proved successful for investigating highly nonlinear partially observed dynamic systems of low dimension arising in analysis of epidemiological and ecological population dynamics (Bretó,

2018; Pons-Salort and Grassly, 2018; de Cellès et al., 2018; Marino et al., 2019). This article develops a methodological extension motivated by the analysis of interacting biological populations. Similar challenges related to nonlinear non-Gaussian dynamic models arise in geophysical modeling. Relative to biological systems, geophysical applications are characterized by a greater number of spatial locations, better mathematical understanding of the underlying processes, and lower stochasticity. From this literature, the locally weighted particle filter of Poterjoy (2016) is perhaps closest to our approach, but the local weights of Poterjoy (2016) are used to construct a localized Kalman gain which is motivated by a Gaussian approximation comparable to EnKF. EnKF arose originally via geophysical research (Evensen and van Leeuwen, 1996) and has since become used more widely for inference on SpatPOMP models (Katzfuss et al., 2020; Lei et al., 2010). However, EnKF can fail entirely even on simple POMP models if the structure is sufficiently non-Gaussian. For example, let X_n be a one-dimensional Gaussian random walk, and let Y_n given $X_n = x_n$ be normally distributed with mean 0 and variance x_n^2 . The linear filter rule used by EnKF to update the estimate of X_n given Y_n has mean zero for any value of X_n , since X_n and Y_n are uncorrelated. Therefore, the EnKF filter estimate of the latent process remains essentially constant regardless of the data. Models of this form are used in finance to describe stochastic volatility. EnKF could be applied more successfully by modifying model, such as replacing Y_n by $|Y_n|$, but for complex models it may be unclear whether and where such problems are arising. Our results show that there is room for improvement over EnKF on a spatiotemporal epidemiology model, though in our example there is no clear advantage for BF methods over BPF.

Latent state trajectories constructed in our BF algorithms are all generated from the model simulator, appropriately reweighted and resampled, and so they are necessarily valid sample paths of the model. For example, spatial smoothness properties of the model through space, or conservation properties where some function of the system remains unchanged through time, are maintained in the BF trajectories. This is not generally true for the block particle filter (since resampling blocks can lead to violations at block boundaries) or for EnKF (since the filter procedure perturbs particles using a linear update rule that cannot

respect nonlinear relationships). The practical importance of smoothness and conservation considerations will vary with the system under investigation, but this property of BF gives the scientific investigator one less thing to worry about.

The algorithms UBF, ABF, ABF-IR, GIRF, PF, BPF, and EnKF compared in this article all enjoy the plug-and-play property, facilitating their implementations in general-purpose software. The numerical results for this paper use the `abf`, `abfir`, `girf`, `pfilter`, `bpfilter` and `enkf` functions via the open-source R package `spatPomp` (Asfaw et al., 2021b) that provides a spatiotemporal extension of the R package `pomp` (King et al., 2016). UBF was implemented using `abf` with $J = 1$ particles per replicate. The source code for this paper will be contributed to an open-source scientific archive upon acceptance for publication.

References

- Ades, M. and Van Leeuwen, P. J. (2015). The equivalent-weights particle filter in a high-dimensional system. *Quarterly Journal of the Royal Meteorological Society*, 141(687):484–503.
- Asfaw, K., Ionides, E. L., and King, A. A. (2021a). `spatPomp`: R package for statistical inference for spatiotemporal partially observed Markov processes. <https://github.com/kidusasfaw/spatPomp>.
- Asfaw, K., Park, J., Ho, A., King, A. A., and Ionides, E. L. (2021b). Statistical inference for spatiotemporal partially observed Markov processes via the R package `spatpomp`. *arXiv:2101.01157*.
- Becker, A. D., Zhou, S. H., Wesolowski, A., and Grenfell, B. T. (2020). Coexisting attractors in the context of cross-scale population dynamics: Measles in London as a case study. *Proceedings of the Royal Society of London, Series B*, 287(1925):20191510.
- Bengtsson, T., Bickel, P., and Li, B. (2008). Curse-of-dimensionality revisited: Collapse of the particle filter in very large scale systems. In Speed, T. and Nolan, D., editors,

- Probability and Statistics: Essays in Honor of David A. Freedman*, pages 316–334. Institute of Mathematical Statistics, Beachwood, OH.
- Bentkus, V., Götze, F., and Tikhomirov, A. (1997). Berry–Esseen bounds for statistics of weakly dependent samples. *Bernoulli*, 3(3):329–349.
- Beskos, A., Crisan, D., Jasra, A., Kamatani, K., and Zhou, Y. (2017). A stable particle filter for a class of high-dimensional state-space models. *Advances in Applied Probability*, 49(1):24–48.
- Bjørnstad, O. N. and Grenfell, B. T. (2001). Noisy clockwork: Time series analysis of population fluctuations in animals. *Science*, 293:638–643.
- Brehmer, J., Louppe, G., Pavez, J., and Cranmer, K. (2020). Mining gold from implicit models to improve likelihood-free inference. *Proceedings of the National Academy of Sciences of the USA*, 117(10):5242–5249.
- Breiman, L. (1996). Bagging predictors. *Machine learning*, 24(2):123–140.
- Bretó, C. (2018). Modeling and inference for infectious disease dynamics: A likelihood-based approach. *Statistical Science*, 33(1):57–69.
- Bretó, C., He, D., Ionides, E. L., and King, A. A. (2009). Time series analysis via mechanistic models. *Annals of Applied Statistics*, 3:319–348.
- Bretó, C. and Ionides, E. L. (2011). Compound Markov counting processes and their applications to modeling infinitesimally over-dispersed systems. *Stochastic Processes and their Applications*, 121:2571–2591.
- Chandler, R. E. (2013). Exploiting strength, discounting weakness: Combining information from multiple climate simulators. *Philosophical Transactions of the Royal Society A: Mathematical, Physical and Engineering Sciences*, 371(1991):20120388.

- de Cellès, M. D., Magpantay, F. M., King, A. A., and Rohani, P. (2018). The impact of past vaccination coverage and immunity on pertussis resurgence. *Science Translational Medicine*, 10(434):eaa1748.
- Del Moral, P., Moulines, E., Olsson, J., and Vergé, C. (2017). Convergence properties of weighted particle islands with application to the double bootstrap algorithm. *Stochastic Systems*, 6(2):367–419.
- Del Moral, P. and Murray, L. M. (2015). Sequential Monte Carlo with highly informative observations. *Journal on Uncertainty Quantification*, 3:969–997.
- Doucet, A., de Freitas, N., and Gordon, N. J. (2001). *Sequential Monte Carlo Methods in Practice*. Springer, New York.
- Doucet, A. and Johansen, A. (2011). A tutorial on particle filtering and smoothing: Fifteen years later. In Crisan, D. and Rozovsky, B., editors, *Oxford Handbook of Nonlinear Filtering*. Oxford University Press.
- Ebert, E. E. (2001). Ability of a poor man’s ensemble to predict the probability and distribution of precipitation. *Monthly Weather Review*, 129(10):2461–2480.
- Evensen, G. and van Leeuwen, P. J. (1996). Assimilation of geostat altimeter data for the Agulhas Current using the ensemble Kalman filter with a quasigeostrophic model. *Monthly Weather Review*, 124:58–96.
- Gordon, N., Salmond, D. J., and Smith, A. F. M. (1993). Novel approach to nonlinear/non-Gaussian Bayesian state estimation. *IEE Proceedings-F*, 140(2):107–113.
- He, D., Ionides, E. L., and King, A. A. (2010). Plug-and-play inference for disease dynamics: Measles in large and small towns as a case study. *Journal of the Royal Society Interface*, 7:271–283.
- Ionides, E. L., Breto, C., Park, J., Smith, R. A., and King, A. A. (2017). Monte Carlo profile confidence intervals for dynamic systems. *Journal of the Royal Society Interface*, 14:1–10.

- Ionides, E. L., Nguyen, D., Atchadé, Y., Stoev, S., and King, A. A. (2015). Inference for dynamic and latent variable models via iterated, perturbed Bayes maps. *Proceedings of the National Academy of Sciences of the USA*, 112(3):719—724.
- Jirak, M. (2016). Berry–Esseen theorems under weak dependence. *The Annals of Probability*, 44(3):2024–2063.
- Katzfuss, M., Stroud, J. R., and Wikle, C. K. (2020). Ensemble Kalman methods for high-dimensional hierarchical dynamic space-time models. *Journal of the American Statistical Association*, 115(530):866–885.
- Kevrekidis, I. G. and Samaey, G. (2009). Equation-free multiscale computation: Algorithms and applications. *Annual Review of Physical Chemistry*, 60:321–344.
- King, A. A., Ionides, E. L., Pascual, M., and Bouma, M. J. (2008). Inapparent infections and cholera dynamics. *Nature*, 454:877–880.
- King, A. A., Nguyen, D., and Ionides, E. L. (2016). Statistical inference for partially observed Markov processes via the R package pomp. *Journal of Statistical Software*, 69:1–43.
- Lei, J., Bickel, P., and Snyder, C. (2010). Comparison of ensemble Kalman filters under non-Gaussianity. *Monthly Weather Review*, 138(4):1293–1306.
- Leutbecher, M. and Palmer, T. N. (2008). Ensemble forecasting. *Journal of Computational Physics*, 227(7):3515–3539.
- Li, R., Pei, S., Chen, B., Song, Y., Zhang, T., Yang, W., and Shaman, J. (2020). Substantial undocumented infection facilitates the rapid dissemination of novel coronavirus (SARS-CoV-2). *Science*, 368(6490):489–493.
- Marino, J. A., Peacor, S. D., Bunnell, D. B., Vanderploeg, H. A., Pothoven, S. A., Elgin, A. K., Bence, J. R., Jiao, J., and Ionides, E. L. (2019). Evaluating consumptive and nonconsumptive predator effects on prey density using field times series data. *Ecology*, 100(3):e02583.

- Ng, B., Peshkin, L., and Pfeffer, A. (2002). Factored particles for scalable monitoring. *Proceedings of the 18th Conference on Uncertainty and Artificial Intelligence*, pages 370–377.
- Ning, N., Ionides, E. L., and Ritov, Y. (2021). Scalable Monte Carlo inference and rescaled local asymptotic normality. *Bernoulli*, pre-published online.
- Palmer, T. N. (2002). The economic value of ensemble forecasts as a tool for risk assessment: From days to decades. *Quarterly Journal of the Royal Meteorological Society*, 128(581):747–774.
- Park, J. and Ionides, E. L. (2019). Inference on high-dimensional implicit dynamic models using a guided intermediate resampling filter. *Arxiv:1708.08543v3*.
- Park, J. and Ionides, E. L. (2020). Inference on high-dimensional implicit dynamic models using a guided intermediate resampling filter. *Statistics & Computing*, 30:1497–1522.
- Pitt, M. K. and Shepard, N. (1999). Filtering via simulation: Auxillary particle filters. *Journal of the American Statistical Association*, 94:590–599.
- Pons-Salort, M. and Grassly, N. C. (2018). Serotype-specific immunity explains the incidence of diseases caused by human enteroviruses. *Science*, 361(6404):800–803.
- Poterjoy, J. (2016). A localized particle filter for high-dimensional nonlinear systems. *Monthly Weather Review*, 144(1):59–76.
- Rebeschini, P. and van Handel, R. (2015). Can local particle filters beat the curse of dimensionality? *The Annals of Applied Probability*, 25(5):2809–2866.
- Snyder, C., Bengtsson, T., and Morzfeld, M. (2015). Performance bounds for particle filters using the optimal proposal. *Monthly Weather Review*, 143(11):4750–4761.
- Xia, Y., Bjørnstad, O. N., and Grenfell, B. T. (2004). Measles metapopulation dynamics: A gravity model for epidemiological coupling and dynamics. *American Naturalist*, 164(2):267–281.

Supplement to “Bagged filters for partially observed interacting systems”

E. L. Ionides, K. Asfaw, J. Park and A. A. King

June 30, 2021

Supplementary Content

S1	A generalization to models without latent unit structure	2
S2	Adapted simulation for an Euler approximation	3
S3	UBF convergence: Proof of Theorem 1	6
S4	ABF and ABF-IR convergence: Proof of Theorem 2	10
S5	The correlated Brownian motion example	19
S6	The measles example	21
S7	Varying the neighborhood for measles	23
S8	A Lorenz-96 example	24
S9	A memory-efficient representation of ABF	27
S10	Bagged filters for functions of the latent states	28
S11	An iterated bagged filter for parameter estimation	31
S12	Replicates versus particles for the measles model	33

S1 A generalization to models without latent unit structure

Variations of the algorithms in the main text apply when there is no latent unit structure. In this case, the observation vector $\mathbf{Y}_n = (Y_{1,n}, \dots, Y_{U,n})$ consists of a collection of measurements on a general latent vector X_n . We may have the structure that $Y_{1,n}, \dots, Y_{U,n}$ are conditionally independent given X_n , but even this is not essential to the approach. This is most readily seen in the context of the unadapted bagged filter, giving rise to the generalized unadapted bagged filter (G-UBF) algorithm defined as follows.

Algorithm G-UBF (Generalized unadapted bagged filter).

input:

Simulator for $f_{X_n|X_{n-1}}(x_n|x_{n-1})$

Evaluator for $f_{Y_{u,n}|X_n}(y_{u,n}^*|x_n)$

Number of bootstrap filters, \mathcal{I}

Neighborhood structure, $B_{u,n}$, for $u \in 1:U$ and $n \in 1:N$

Data, $y_{u,n}^*$ for $u \in 1:U$ and $n \in 1:N$

output:

Log likelihood estimate, $\ell^{\text{MC}} = \sum_{n=1}^N \sum_{u=1}^U \ell_{u,n}^{\text{MC}}$

For i in $1:\mathcal{I}$

simulate $X_{n,i}^{\text{sim}}$ from the dynamic model, for $n \in 1:N$

End For

Prediction weights, $w_{u,n,i}^P = f_{Y_{B_{u,n}}|X_{1:n}}(y_{B_{u,n}}^* | X_{1:n,i}^{\text{sim}})$

Measurement weights, $w_{u,n,i}^M = f_{Y_{u,n}|X_n, Y_{B_{u,n}}}(y_{u,n}^* | X_{n,i}^{\text{sim}}, y_{B_{u,n}}^*)$

Conditional log likelihood estimate, $\ell_{u,n}^{\text{MC}} = \log \left(\sum_{i=1}^{\mathcal{I}} w_{u,n,i}^M w_{u,n,i}^P \right) - \log \left(\sum_{\tilde{i}=1}^{\mathcal{I}} w_{u,n,\tilde{i}}^P \right)$

The algorithm G-UBF operates on an arbitrary POMP model. G-UBF therefore provides a potential approach to extending methodologies from SpatPOMP models to models that have some similarity to a SpatPOMP without formally meeting the definition. For example, there may be collections of interacting processes at different spatial scales in a spatiotemporal system. Alternatively, the potential outcomes of the latent process may vary between spatial units, such as when modeling interactions between terrestrial and aquatic ecosystems. We do not further explore G-UBF here.

S2 Adapted simulation for an Euler approximation

We investigate the adapted simulation process by considering a continuous-time limit where it becomes a diffusion process. We find that adapted simulation can effectively track the latent process when the measurement error is on an appropriate scale. However, when the measurement error is large compared to the latent process noise, adapted simulation can fail in situations where filtering succeeds. We work with a one-dimensional POMP model having a latent process constructed as an Euler approximation,

$$X_{n+1} = X_n + \mu(X_n)\delta + \sigma\sqrt{\delta}\epsilon_{n+1}, \quad (\text{S1})$$

which provides a numerical solution to a one-dimensional stochastic differential equation,

$$dX(t) = \mu(X(t)) dt + \sigma dU(t),$$

where $\{U(t)\}$ is a standard Brownian motion. We will consider several different measurement processes.

S2.1 Measurement error on the same scale as the process noise

Here, we consider the measurement model

$$Y_{n+1} = \mu(X_n)\delta + \sigma\sqrt{\delta}\epsilon_{n+1} + \tau\sqrt{\delta}\eta_{n+1}. \quad (\text{S2})$$

This is an approximation to the increment $Y(t+\delta) - Y(t)$ of a continuous time measurement model

$$dY(t) = dX(t) + \tau dV(t), \quad (\text{S3})$$

where $\{V(t)\}$ is a standard Brownian motion independent of $\{U(t)\}$. The measurement model (S3) makes inference on $X(t)$ given $Y(t)$ a continuous time version of the filtering problem. A feature of this model is that $Y(t)$ does not directly track the level of the state, since the solution with initial conditions $Y(t_0) = X(t_0)$ and $V(t_0) = 0$ is

$$Y(t) = X(t) + \tau V(t).$$

The measurement error, $\tau V(t)$, has variance $\tau^2 t$ that increases with t . However, under appropriate conditions, information on changes in $\{X(t)\}$ obtained via $\{Y(t)\}$ are enough to track $X(t)$ indirectly via the filtering equations. For the POMP given by (S1) and (S2), we can calculate exactly the adapted simulation distribution $f_{X_{n+1}|Y_{n+1}, X_n}$. It is convenient to work conditionally on X_n , allowing us to treat X_n and $\mu(X_n)$ as constants, with X_{n+1} and Y_{n+1} therefore being jointly normally distributed. A Gaussian distribution calculation then gives the conditional moments. First, we find

$$\begin{aligned} \mathbb{E}[X_{n+1}|Y_{n+1}, X_n] &= X_n + \mu(X_n)\delta + \mathbb{E}[\sigma\sqrt{\delta}\epsilon_{n+1} \mid \sigma\sqrt{\delta}\epsilon_{n+1} + \tau\sqrt{\delta}\eta_{n+1}] \\ &= X_n + \mu(X_n)\delta + \frac{\sigma^2}{\sigma^2 + \tau^2}(\sigma\sqrt{\delta}\epsilon_{n+1} + \tau\sqrt{\delta}\eta_{n+1}) \\ &= X_n + \mu(X_n)\delta + \frac{\sigma^2}{\sigma^2 + \tau^2}(Y_{n+1} - \mu(X_n)\delta). \end{aligned}$$

Then,

$$\begin{aligned}
\text{Var}[X_{n+1} | Y_{n+1}, X_n] &= \text{Var}[\sigma\sqrt{\delta}\epsilon_{n+1} | \sigma\sqrt{\delta}\epsilon_{n+1} + \tau\sqrt{\delta}\eta_{n+1}] \\
&= \sigma^2\delta - \frac{\sigma^4\delta^2}{\sigma^2\delta + \tau^2\delta} \\
&= \delta \frac{\sigma^2\tau^2}{\sigma^2 + \tau^2}.
\end{aligned}$$

Call the adapted simulation process $\{A_n, n = 1, 2, \dots\}$, defined conditionally on $\{Y_n, n = 1, 2, \dots\}$. We see from the above calculation that A_n can be constructed by the recursion

$$\begin{aligned}
A_{n+1} &= A_n + \mu(A_n)\delta + \frac{\sigma^2}{\sigma^2 + \tau^2} \left(\mu(X_n)\delta + \sigma\sqrt{\delta}\epsilon_{n+1} + \tau\sqrt{\delta}\eta_{n+1} - \mu(A_n)\delta \right) \\
&\quad + \frac{\sigma\tau}{\sqrt{\sigma^2 + \tau^2}} \sqrt{\delta}\zeta_{n+1}
\end{aligned}$$

where $\{\zeta_n\}$ is an iid standard normal sequence independent of $\{\epsilon_n, \eta_n\}$. To study how well the adapted simulation tracks $\{X_n\}$, we subtract X_{n+1} from both sides to get

$$\begin{aligned}
[A_{n+1} - X_{n+1}] &= [A_n - X_n] + [\mu(A_n) - \mu(X_n)]\delta - \sigma\sqrt{\delta}\epsilon_{n+1} \\
&\quad + \frac{\sigma^2}{\sigma^2 + \tau^2} \left([\mu(X_n) - \mu(A_n)]\delta + \sigma\sqrt{\delta}\epsilon_{n+1} + \tau\sqrt{\delta}\eta_{n+1} \right) + \frac{\sigma\tau}{\sqrt{\sigma^2 + \tau^2}} \sqrt{\delta}\zeta_{n+1} \\
&= [A_n - X_n] + \frac{2\sigma^2 + \tau^2}{\sigma^2 + \tau^2} [\mu(X_n) - \mu(A_n)]\delta \\
&\quad + \frac{\sigma^2\tau\sqrt{\delta}\eta_{n+1} - \sigma\tau^2\sqrt{\delta}\epsilon_{n+1}}{\sigma^2 + \tau^2} + \frac{\sigma\tau}{\sqrt{\sigma^2 + \tau^2}} \sqrt{\delta}\zeta_{n+1}.
\end{aligned}$$

A_n tracks X_n when the process $\{A_n - X_n, n = 1, 2, \dots\}$ is stable. This happens when $\mu(x) - \mu(y)$ is negative when x is sufficiently larger than y . For example, a stable autoregressive process with $\mu(x) = -ax$ gives a stable adapted filter process.

S2.2 Independent measurement error on a scale that gives a finite limiting amount of information about $X(t)$ from measurements on a unit time interval

We now consider the measurement model

$$\begin{aligned}
Y_{n+1} &= X_{n+1} + \frac{\tau}{\sqrt{\delta}}\eta_{n+1} \\
&= X_n + \mu(X_n)\delta + \sigma\sqrt{\delta}\epsilon_{n+1} + \frac{\tau}{\sqrt{\delta}}\eta_{n+1},
\end{aligned} \tag{S4}$$

where $\{\epsilon_n, \eta_n\}$ is a collection of independent standard normal random variables. The conditional mean is now

$$\begin{aligned}
\mathbb{E}[X_{n+1} | Y_{n+1}, X_n] &= X_n + \mu(X_n)\delta + \mathbb{E}\left[\sigma\sqrt{\delta}\epsilon_{n+1} \mid \sigma\sqrt{\delta}\epsilon_{n+1} + \frac{\tau}{\sqrt{\delta}}\eta_{n+1}\right] \\
&= X_n + \mu(X_n)\delta + \frac{\sigma^2\delta}{\sigma^2\delta + \tau^2/\delta} (\sigma\sqrt{\delta}\epsilon_{n+1} + \tau\sqrt{\delta}\eta_{n+1})
\end{aligned} \tag{S5}$$

Using (S4) and (S5) gives

$$\mathbb{E}[X_{n+1}|Y_{n+1}, X_n] = X_n + \mu(X_n)\delta + \frac{\sigma^2\delta^2}{\sigma^2\delta^2 + \tau^2} (Y_{n+1} - X_n - \mu(X_n)\delta).$$

In the limit as $\delta \rightarrow 0$, the contribution from the measurement is order δ^2 and is therefore negligible. Although the observation process is meaningfully informative about the latent process, the adapted simulation fails to track the latent process in this limit. Intuitively, this is because the adapted simulation is trying to track differences in the latent process, but for this model the signal to noise ratio for the difference in each interval of length δ tends to zero.

S2.3 Independent measurements of the latent process with measurement error on a scale that gives a useful adapted process as $\delta \rightarrow 0$

We now consider the measurement model

$$\begin{aligned} Y_{n+1} &= X_{n+1} + \tau\eta_{n+1} \\ &= X_n + \mu(X_n)\delta + \sigma\sqrt{\delta}\epsilon_{n+1} + \tau\eta_{n+1}. \end{aligned} \tag{S6}$$

The conditional mean is now

$$\begin{aligned} \mathbb{E}[X_{n+1}|Y_{n+1}, X_n] &= X_n + \mu(X_n)\delta + \mathbb{E}[\sigma\sqrt{\delta}\epsilon_{n+1} | \sigma\sqrt{\delta}\epsilon_{n+1} + \tau\eta_{n+1}] \\ &= X_n + \mu(X_n)\delta + \frac{\sigma^2\delta}{\sigma^2\delta + \tau^2} (\sigma\sqrt{\delta}\epsilon_{n+1} + \tau\eta_{n+1}) \end{aligned} \tag{S7}$$

Using (S6) and (S7) gives

$$\begin{aligned} \mathbb{E}[X_{n+1}|Y_{n+1}, X_n] &= X_n + \mu(X_n)\delta + \frac{\sigma^2\delta}{\sigma^2\delta + \tau^2} (Y_{n+1} - X_n - \mu(X_n)\delta) \\ &= X_n + \mu(X_n)\delta + \frac{\sigma^2}{\tau^2}\delta (Y_{n+1} - X_n - \mu(X_n)\delta) + o(\delta) \end{aligned}$$

In the limit as $\delta \rightarrow 0$, the adapted simulation has a diffusive drift toward the value of the latent process.

For disease models, incidence data can arguably be considered as noisy measurements of the change of a state variable (number of susceptibles) that is not directly measured. This could correspond to a situation where the measurement error is on the same scale as the process noise (Subsection S2.1). Alternatively, we could think of weekly aggregated incidence as a noisy measurement of the infected class, in which case the measurement error could match the scaling in Subsection S2.3.

The model in Subsection S2.2 is a cautionary tale, warning us against carrying out adapted simulation on short time intervals. An interpretation is that one should not carry out adapted simulation unless a reasonable amount of information has accrued. When each observation has low information, a particle filter may enable solution to the filtering problem without particle depletion. It is when the data are highly informative that the curse of dimensionality makes basic particle filters ineffective, opening up demand for alternative methods.

We are now in a better position to understand why it may be appropriate to keep many particle representations at intermediate timesteps while resampling down to a single representative at each

observation time, as ABF and ABF-IR do. We have seen that adaptive simulation can fail when observations occur frequently. Resampling down to a single particle too often can lose the ability for the adapted process to track the latent process. This implies that adapted simulation should not be relied upon more than necessary to ameliorate the curse of dimensionality: once proper importance sampling for filtering problem becomes tractable in a sufficiently small spatiotemporal neighborhood, one should maintain weighted particles on this spatiotemporal scale rather than resorting to adapted simulation.

S3 UBF convergence: Proof of Theorem 1

We consider a collection of models $f_{\mathbf{x}_{0:N}, \mathbf{y}_{1:N}}$ and data $\mathbf{y}_{1:N}^*$ defined for each (U, N) . These models and datasets are not required to have any nesting relationship, so we do not insist that $X_{1,1}$ or $y_{1,1}^*$ should be the same for $(U, N) = (10, 10)$ as for $(U, N) = (100, 100)$. Formally, we define probability and expectation on a product space of the stochastic model and Monte Carlo outcomes. Monte Carlo quantities such as the output of the UBF, ABF and ABF-IR algorithms depend on the data but not on any random variables constructed under the model. As a consequence, we can use \mathbb{E} to correspond both to expectations over Monte Carlo stochasticity (for Monte Carlo quantities) and model stochasticity (for random variables constructed under the model). We suppress discussion of measurability by assuming that all functions considered have appropriate measurability properties. We restate the assumptions and statement for Theorem 1.

Assumption A1. *There is an $\epsilon_{A1} > 0$, independent of U and N , and a collection of neighborhoods $\{B_{u,n} \subset A_{u,n}, u \in 1:U, n \in 1:N\}$ such that, for all u and n , any bounded real-valued function $|h(x)| \leq 1$, and any value of $x_{B_{u,n}^c}$,*

$$\left| \int h(x_{u,n}) f_{X_{u,n}|Y_{B_{u,n}}, X_{B_{u,n}^c}}(x_{u,n} | y_{B_{u,n}}^*, x_{B_{u,n}^c}) dx_{u,n} - \int h(x_{u,n}) f_{X_{u,n}|Y_{B_{u,n}}}(x_{u,n} | y_{B_{u,n}}^*) dx_{u,n} \right| < \epsilon_{A1}. \quad (\text{S8})$$

We use the total variation bound in Assumption A1 via the following Proposition S1, which replaces conditioning on $X_{B_{u,n}^c}$ with conditioning on $Y_{B_{u,n}^c}$. The bound in (S9) could be used in place of Assumption A1.

Proposition S1. *Under the conditions of Assumption A1, (S8) implies*

$$\left| \int h(x_{u,n}) f_{X_{u,n}|Y_{A_{u,n}}}(x_{u,n} | y_{A_{u,n}}^*) dx_{u,n} - \int h(x_{u,n}) f_{X_{u,n}|Y_{B_{u,n}}}(x_{u,n} | y_{B_{u,n}}^*) dx_{u,n} \right| < \epsilon_{A1} \quad (\text{S9})$$

Proof. For notational compactness, we suppress the arguments $x_{u,n}$, $x_{B_{u,n}^c}$, $y_{A_{u,n}}^*$, $y_{B_{u,n}}^*$ matching the subscripts of conditional densities. Using the conditional independence of the measurements

given the latent process, we calculate

$$\begin{aligned}
& \left| \int h(x_{u,n}) f_{X_{u,n}|Y_{A_{u,n}}} dx_{u,n} - \int h(x_{u,n}) f_{X_{u,n}|Y_{B_{u,n}}} dx_{u,n} \right| \\
&= \left| \int \left\{ \int h(x_{u,n}) f_{X_{u,n}|Y_{B_{u,n}}, X_{B_{\tilde{u},n}^c}} dx_{u,n} - \int h(x_{u,n}) f_{X_{u,n}|Y_{B_{u,n}}} dx_{u,n} \right\} f_{X_{B_{\tilde{u},n}^c}|Y_{A_{u,n}}} dx_{B_{\tilde{u},n}^c} \right| \\
&\leq \int \left| \int h(x_{u,n}) f_{X_{u,n}|Y_{B_{u,n}}, X_{B_{\tilde{u},n}^c}} dx_{u,n} - \int h(x_{u,n}) f_{X_{u,n}|Y_{B_{u,n}}} dx_{u,n} \right| f_{X_{B_{\tilde{u},n}^c}|Y_{A_{u,n}}} dx_{B_{\tilde{u},n}^c} \\
&< \int \epsilon_{A1} f_{X_{B_{\tilde{u},n}^c}|Y_{A_{u,n}}} dx_{B_{\tilde{u},n}^c} = \epsilon_{A1}.
\end{aligned}$$

□

Assumption A2. For the collection of neighborhoods in Assumption A1, with $B_{u,n}^+ = B_{u,n} \cup (u, n)$, there is a constant b , depending on ϵ_{A1} but not on U and N , such that

$$\sup_{u \in 1:U, n \in 1:N} |B_{u,n}^+| \leq b.$$

Assumption A3. There is a constant Q , independent of U and N , such that, for all u and n ,

$$Q^{-1} < f_{Y_{u,n}|X_{u,n}}(y_{u,n}^* | x_{u,n}) < Q$$

Assumption A4. There exists $\epsilon_{A4} > 0$, independent of U and N , such that the following holds. For each u, n , a set $C_{u,n} \subset (1:U) \times (0:N)$ exists such that $(\tilde{u}, \tilde{n}) \notin C_{u,n}$ implies $B_{u,n}^+ \cap B_{\tilde{u},\tilde{n}}^+ = \emptyset$ and

$$\left| f_{X_{B_{\tilde{u},\tilde{n}}^+}|X_{B_{u,n}^+}} - f_{X_{B_{u,n}^+}} \right| < \epsilon_{A4} f_{X_{B_{\tilde{u},\tilde{n}}^+}} \quad (\text{S10})$$

Further, there is a uniform bound $|C_{u,n}| \leq c$.

Assumption A4 is needed only to ensure that the variance bound in Theorem 1 is essentially $O(UN)$ rather than $O(U^2N^2)$. Both these rates avoid the exponentially increasing variance characterizing the curse of dimensionality. Lower variance than $O(UN)$ cannot be anticipated for any sequential Monte Carlo method since the log likelihood estimate can be written as a sum of UN terms each of which involves its own sequential Monte Carlo calculation.

Theorem 1. Let ℓ^{MC} denote the Monte Carlo likelihood approximation constructed by UBF. Consider a limit with a growing number of bootstrap replicates, $\mathcal{I} \rightarrow \infty$, and suppose assumptions A1, A2 and A3. There are quantities $\epsilon(U, N)$ and $V(U, N)$, with bounds $|\epsilon| < \epsilon_{A1} Q^2$ and $V < Q^{4b} U^2 N^2$, such that

$$\mathcal{I}^{1/2} [\ell^{MC} - \ell - \epsilon UN] \xrightarrow[\mathcal{I} \rightarrow \infty]{d} \mathcal{N}[0, V], \quad (\text{S11})$$

where $\xrightarrow[\mathcal{I} \rightarrow \infty]{d}$ denotes convergence in distribution and $\mathcal{N}[\mu, \Sigma]$ is the normal distribution with mean μ and variance Σ . If additionally Assumption A4 holds, we obtain an improved variance bound

$$V < Q^{4b} UN (c + \epsilon_{A4} (UN - c)). \quad (\text{S12})$$

Proof. Suppose the quantities $w_{u,n,i}^M$ and $w_{u,n,i}^P$ constructed in Algorithm UBF are considered i.i.d. replicates of jointly defined random variables $w_{u,n}^M$ and $w_{u,n}^P$, for each $(u, n) \in 1:U \times 1:N$. Also, write

$$\Delta_{u,n}^{MP} = \frac{1}{\sqrt{\mathcal{I}}} \sum_{i=1}^{\mathcal{I}} (w_{u,n,i}^M w_{u,n,i}^P - \mathbb{E}[w_{u,n}^M w_{u,n}^P]), \quad \Delta_{u,n}^P = \frac{1}{\sqrt{\mathcal{I}}} \sum_{i=1}^{\mathcal{I}} (w_{u,n,i}^P - \mathbb{E}[w_{u,n}^P]),$$

Then, using the delta method (e.g., Section 2.5.3 in Liu (2001)) we find

$$\begin{aligned} \ell_{u,n}^{\text{MC}} &= \log \left(\frac{\sum_{i=1}^{\mathcal{I}} w_{u,n,i}^M w_{u,n,i}^P}{\sum_{i=1}^{\mathcal{I}} w_{u,n,i}^P} \right) \\ &= \log \left(\mathbb{E}[w_{u,n}^M w_{u,n}^P] + \mathcal{I}^{-1/2} \Delta_{u,n}^{MP} \right) - \log \left(\mathbb{E}[w_{u,n}^P] + \mathcal{I}^{-1/2} \Delta_{u,n}^P \right) \\ &= \log \left(\frac{\mathbb{E}[w_{u,n}^M w_{u,n}^P]}{\mathbb{E}[w_{u,n}^P]} \right) + \mathcal{I}^{-1/2} \left(\frac{\Delta_{u,n}^{MP}}{\mathbb{E}[w_{u,n}^M w_{u,n}^P]} - \frac{\Delta_{u,n}^P}{\mathbb{E}[w_{u,n}^P]} \right) + o_P(\mathcal{I}^{-1/2}) \end{aligned} \quad (\text{S13})$$

The joint distribution of $\{(\Delta_{u,n}^{MP}, \Delta_{u,n}^P), (u, n) \in 1:U \times 1:N\}$ follows a standard central limit theorem as $\mathcal{I} \rightarrow \infty$. Each term has mean zero, with covariances uniformly bounded over $(u, n, \tilde{u}, \tilde{n})$ due to Assumption A3. Specifically,

$$\text{Var} \begin{pmatrix} \Delta_{u,n}^{MP} \\ \Delta_{u,n}^P \\ \Delta_{\tilde{u},\tilde{n}}^{MP} \\ \Delta_{\tilde{u},\tilde{n}}^P \end{pmatrix} = \begin{pmatrix} \text{Var}(w_{u,n}^M w_{u,n}^P) & \text{Cov}(w_{u,n}^M w_{u,n}^P, w_{u,n}^P) & \text{Cov}(w_{u,n}^M w_{u,n}^P, w_{\tilde{u},\tilde{n}}^M w_{\tilde{u},\tilde{n}}^P) & \text{Cov}(w_{u,n}^M w_{u,n}^P, w_{\tilde{u},\tilde{n}}^P) \\ \text{Cov}(w_{u,n}^M w_{u,n}^P, w_{u,n}^P) & \text{Var}(w_{u,n}^P) & \text{Cov}(w_{u,n}^P, w_{\tilde{u},\tilde{n}}^M w_{\tilde{u},\tilde{n}}^P) & \text{Cov}(w_{u,n}^P, w_{\tilde{u},\tilde{n}}^P) \\ \text{Cov}(w_{u,n}^M w_{u,n}^P, w_{\tilde{u},\tilde{n}}^M w_{\tilde{u},\tilde{n}}^P) & \text{Cov}(w_{u,n}^P, w_{\tilde{u},\tilde{n}}^M w_{\tilde{u},\tilde{n}}^P) & \text{Var}(w_{\tilde{u},\tilde{n}}^M w_{\tilde{u},\tilde{n}}^P) & \text{Cov}(w_{\tilde{u},\tilde{n}}^M w_{\tilde{u},\tilde{n}}^P, w_{\tilde{u},\tilde{n}}^P) \\ \text{Cov}(w_{u,n}^M w_{u,n}^P, w_{\tilde{u},\tilde{n}}^P) & \text{Cov}(w_{u,n}^P, w_{\tilde{u},\tilde{n}}^P) & \text{Cov}(w_{\tilde{u},\tilde{n}}^M w_{\tilde{u},\tilde{n}}^P, w_{\tilde{u},\tilde{n}}^P) & \text{Var}(w_{\tilde{u},\tilde{n}}^P) \end{pmatrix}$$

Note that

$$\begin{aligned} \log \left[\frac{\mathbb{E}[w_{u,n}^M w_{u,n}^P]}{\mathbb{E}[w_{u,n}^P]} \right] &= \log \left[\frac{\int f_{Y_{u,n}|X_{u,n}}(y_{u,n}^* | x_{u,n,i}) f_{Y_{B_{u,n}}|X_{B_{u,n}}}(y_{B_{u,n}}^* | x_{B_{u,n}}) f_{X_{B_{u,n}^+}}(x_{B_{u,n}^+}) dx_{B_{u,n}^+}}{\int f_{Y_{B_{u,n}}|X_{B_{u,n}}}(y_{B_{u,n}}^* | x_{B_{u,n}}) f_{X_{B_{u,n}}}(x_{B_{u,n}}) dx_{B_{u,n}}} \right] \\ &= \log [f_{Y_{u,n}|Y_{B_{u,n}}}(y_{u,n}^* | y_{B_{u,n}}^*)], \end{aligned}$$

where $B_{u,n}^+ = B_{u,n} \cup (u, n)$. Now, define

$$\Delta_{u,n}^\ell = \left(\frac{\Delta_{u,n}^{MP}}{\mathbb{E}[w_{u,n}^M w_{u,n}^P]} - \frac{\Delta_{u,n}^P}{\mathbb{E}[w_{u,n}^P]} \right)$$

Summing over all $(u, n) \in 1:U \times 1:N$, we get

$$\sqrt{\mathcal{I}} \left(\ell^{\text{MC}} - \sum_{(u,n) \in 1:U \times 1:N} \log f_{Y_{u,n}|Y_{B_{u,n}}}(y_{u,n}^* | y_{B_{u,n}}^*) \right) = \sum_{(u,n) \in 1:U \times 1:N} \Delta_{u,n}^\ell + o(1). \quad (\text{S14})$$

Now,

$$\text{Cov}(\Delta_{u,n}^\ell, \Delta_{\tilde{u},\tilde{n}}^\ell) = \text{Cov} \left(\frac{w_{u,n}^M w_{u,n}^P}{\mathbb{E}[w_{u,n}^M w_{u,n}^P]} - \frac{w_{u,n}^P}{\mathbb{E}[w_{u,n}^P]}, \frac{w_{\tilde{u},\tilde{n}}^M w_{\tilde{u},\tilde{n}}^P}{\mathbb{E}[w_{\tilde{u},\tilde{n}}^M w_{\tilde{u},\tilde{n}}^P]} - \frac{w_{\tilde{u},\tilde{n}}^P}{\mathbb{E}[w_{\tilde{u},\tilde{n}}^P]} \right).$$

Since

$$\left| \frac{w_{u,n}^M w_{u,n}^P}{\mathbb{E}[w_{u,n}^M w_{u,n}^P]} - \frac{w_{u,n}^P}{\mathbb{E}[w_{u,n}^P]} \right| < Q^{2b},$$

we have

$$|\text{Cov}(\Delta_{u,n}^\ell, \Delta_{\tilde{u}, \tilde{n}}^\ell)| < Q^{4b},$$

implying that

$$\text{Var} \left(\sum_{(u,n) \in \mathcal{S}} \Delta_{u,n}^\ell \right) < Q^{4b} U^2 N^2. \quad (\text{S15})$$

If, in addition, (u, n) and $(\tilde{u}, \tilde{n}) \in A_{u,n}$ are sufficiently separated in the sense of Assumption A4, then Lemma S1 shows that Assumption A4 implies

$$|\text{Cov}(\Delta_{u,n}^\ell, \Delta_{\tilde{u}, \tilde{n}}^\ell)| < \epsilon_{A4} Q^{4b}.$$

The number of insufficiently separated neighbors to (u, n) is bounded by c , and so we obtain

$$\text{Var} \left(\sum_{(u,n) \in \mathcal{S}} \Delta_{u,n}^\ell \right) < Q^{4b} UN (c + \epsilon_{A4} (UN - c)). \quad (\text{S16})$$

Now we proceed to bound the bias in the Monte Carlo central limit estimator of ℓ . Putting $h(x_{u,n}) = f_{Y_{u,n}|X_{u,n}}(y_{u,n}^* | x_{u,n})$ into Assumption A1, using Assumption A3, gives

$$|f_{Y_{u,n}|Y_{B_{u,n}}}(y_{u,n}^* | y_{B_{u,n}}^*) - f_{Y_{u,n}|Y_{A_{u,n}}}(y_{u,n}^* | y_{A_{u,n}}^*)| < \epsilon_{A1} Q.$$

Noting that

$$|a - b| < \delta, \quad a > Q^{-1} \text{ and } b > Q^{-1} \text{ implies } |\log(a) - \log(b)| < \delta Q, \quad (\text{S17})$$

we find

$$|\log f_{Y_{u,n}|Y_{B_{u,n}}}(y_{u,n}^* | y_{B_{u,n}}^*) - \log f_{Y_{u,n}|Y_{A_{u,n}}}(y_{u,n}^* | y_{A_{u,n}}^*)| < \epsilon_{A1} Q^2. \quad (\text{S18})$$

Summing over (u, n) , we get

$$\left| \ell - \sum_{(u,n) \in \mathcal{S}} \log f_{Y_{u,n}|Y_{B_{u,n}}}(y_{u,n}^* | y_{B_{u,n}}^*) \right| < \epsilon_{A1} Q^2 UN. \quad (\text{S19})$$

Together, the results in (S14), (S15), (S16) and (S19) confirm the assertions of the theorem. \square

Lemma S1. *Suppose U and V are random variables with joint density satisfying*

$$|f_{V|U}(v | u) - f_V(v)| < \epsilon f_V(v). \quad (\text{S20})$$

Suppose $|g(U)| < a$ and $|h(V)| < b$ for some real-valued function g and h . Then, $\text{Cov}(g(U), h(V)) < abc$.

Proof. The result is obtained by direct calculation, as follows.

$$\begin{aligned}
\text{Cov}(g(U), h(V)) &= \mathbb{E} \left[g(U) \mathbb{E} \left[h(V) - \mathbb{E}[h(V)] \mid U \right] \right] \\
&= \int \left\{ \int g(u) h(v) (f_{V|U}(v|u) - f_V(v)) dv \right\} f_U(u) du \\
&< \int \left\{ \int ab\epsilon f_V(v) dv \right\} f_U(u) du \\
&= ab\epsilon.
\end{aligned}$$

□

S4 ABF and ABF-IR convergence: Proof of Theorem 2

Let $g_{\mathbf{X}_{0:N}, \mathbf{X}_{1:N}^P}(\mathbf{x}_{0:N}, \mathbf{x}_{1:N}^P)$ be the joint density of the adapted process and the proposal process,

$$g_{\mathbf{X}_{0:N}, \mathbf{X}_{1:N}^P}(\mathbf{x}_{0:N}, \mathbf{x}_{1:N}^P) = f_{\mathbf{X}_0}(\mathbf{x}_0) \prod_{n=1}^N f_{\mathbf{X}_n | \mathbf{X}_{n-1}, \mathbf{Y}_n}(\mathbf{x}_n | \mathbf{x}_{n-1}, \mathbf{y}_n^*) f_{\mathbf{X}_n | \mathbf{X}_{n-1}}(\mathbf{x}_n^P | \mathbf{x}_{n-1}). \quad (\text{S21})$$

For $B \subset 1:U \times 1:N$, define $B^{[m]} = B \cap (1:U \times \{m\})$ and set

$$\gamma_B = \prod_{m=1}^N f_{Y_{B^{[m]} | \mathbf{X}_{m-1}}}(y_{B^{[m]}}^* | \mathbf{X}_{m-1}), \quad (\text{S22})$$

using the convention that an empty density f_{Y_\emptyset} evaluates to 1. If we denoting \mathbb{E}_g for expectation for $(\mathbf{X}_{0:N}, \mathbf{X}_{1:N}^P)$ having density $g_{\mathbf{X}_{0:N}, \mathbf{X}_{1:N}^P}$, (S22) can be written as

$$\gamma_B = \mathbb{E}_g \left[f_{Y_B | X_B}(y_B^* | X_B^P) \mid \mathbf{X}_{0:N} \right],$$

so we have

$$\mathbb{E}_g[\gamma_B] = \mathbb{E}_g \left[f_{Y_B | X_B}(y_B^* | X_B^P) \right].$$

Two useful identities are

$$\begin{aligned}
f_{X_{u,n} | Y_{A_{u,n}}}(x_{u,n} | y_{A_{u,n}}^*) &= \frac{\mathbb{E}_g \left[f_{Y_{A_{u,n}} | X_{A_{u,n}}}(y_{A_{u,n}}^* | X_{A_{u,n}}^P) f_{X_{u,n} | X_{A_{u,n}}^{[n]}, \mathbf{X}_{n-1}}(x_{u,n} | X_{A_{u,n}}^{[n]}, \mathbf{X}_{n-1}) \right]}{\mathbb{E}_g \left[f_{Y_{A_{u,n}} | X_{A_{u,n}}}(y_{A_{u,n}}^* | X_{A_{u,n}}^P) \right]}, \\
f_{Y_{u,n} | Y_{A_{u,n}}}(y_{u,n}^* | y_{A_{u,n}}^*) &= \frac{\mathbb{E}_g[\gamma_{A_{u,n}^+}]}{\mathbb{E}_g[\gamma_{A_{u,n}}]}.
\end{aligned}$$

Assumption B1. *There is an $\epsilon_{B1} > 0$, independent of U and N , and a collection of neighborhoods $\{B_{u,n} \subset A_{u,n}, u \in 1:U, n \in 1:N\}$ such that the following holds for all u and n , and any bounded real-valued function $|h(x)| \leq 1$. Setting $A = A_{u,n}$, $B = B_{u,n}$, $f_A(x_A) = f_{Y_A | X_A}(y_A^* | x_A)$, and $f_B(x_B) = f_{Y_B | X_B}(y_B^* | x_B)$, so that we have the identity*

$$f_{X_{u,n} | Y_A}(x | y_A^*) = \frac{\mathbb{E}_g[f_A(X_A^P) f_{X_{u,n} | X_{A^{[n]}}, \mathbf{X}_{n-1}}(x | X_{A^{[n]}}, \mathbf{X}_{n-1})]}{\mathbb{E}_g[f_A(X_A^P)]},$$

we require that

$$\left| \int h(x) \left\{ \frac{\mathbb{E}_g[f_A(X_A^P) f_{X_{u,n}|X_{A^{[n]}}(\mathbf{X}_{n-1})}(x|X_{A^{[n]}}, \mathbf{X}_{n-1})]}{\mathbb{E}_g[f_A(X_A^P)]} - \frac{\mathbb{E}_g[f_B(X_B^P) f_{X_{u,n}|X_{B^{[n]}}(\mathbf{X}_{n-1})}(x|X_{B^{[n]}}, \mathbf{X}_{n-1})]}{\mathbb{E}_g[f_B(X_B^P)]} \right\} dx \right| < \epsilon_{B1}.$$

Assumption B2. The bound $\sup_{u \in 1:U, n \in 1:N} |B_{u,n}^+| \leq b$ in Assumption A2 applies for the neighborhoods defined in Assumption B1. This also implies there is a finite maximum temporal depth for the collection of neighborhoods, defined as

$$d_{\max} = \sup_{(u,n)} \sup_{(\tilde{u}, \tilde{n}) \in B_{u,n}} |n - \tilde{n}|.$$

Assumption B3. Identically to Assumption A3, $Q^{-1} < f_{Y_{u,n}|X_{u,n}}(y_{u,n}^* | x_{u,n}) < Q$.

Proposition S2. Setting $h(x) = f_{Y_{u,n}|X_{u,n}}(y_{u,n}^* | x)$, assumptions B1 and B3 imply

$$\left| \frac{\mathbb{E}_g[\gamma_{A_{u,n}^+}]}{\mathbb{E}_g[\gamma_{A_{u,n}}]} - \frac{\mathbb{E}_g[\gamma_{B_{u,n}^+}]}{\mathbb{E}_g[\gamma_{B_{u,n}}]} \right| < Q\epsilon. \quad (\text{S23})$$

Proof. Using the non-negativity of all terms to justify interchange of integral and expectation,

$$\begin{aligned} & \int h(x) \mathbb{E}_g \left[f_{Y_{B_{u,n}}|X_{B_{u,n}}}(y_{B_{u,n}}^* | X_{B_{u,n}}^P) f_{X_{u,n}|X_{B_{u,n}^{[n]}}(\mathbf{X}_{n-1})}(x|X_{B_{u,n}^{[n]}}, \mathbf{X}_{n-1}) \right] dx \\ &= \mathbb{E}_g \left[\int f_{Y_{u,n}|X_{u,n}}(y_{u,n}^* | x) f_{X_{u,n}|X_{B_{u,n}^{[n]}}(\mathbf{X}_{n-1})}(x|X_{B_{u,n}^{[n]}}, \mathbf{X}_{n-1}) dx \cdot f_{Y_{B_{u,n}}|X_{B_{u,n}}}(y_{B_{u,n}}^* | X_{B_{u,n}}^P) \right] \end{aligned} \quad (\text{S24})$$

But by the construction of g ,

$$\begin{aligned} f_{X_{u,n}|X_{B_{u,n}^{[n]}}(\mathbf{X}_{n-1})}(x|X_{B_{u,n}^{[n]}}, \mathbf{X}_{n-1}) &= g_{X_{u,n}^P|X_{B_{u,n}^{[n]}}(\mathbf{X}_{n-1})}(x|X_{B_{u,n}^{[n]}}, \mathbf{X}_{n-1}) \\ &= g_{X_{u,n}^P|X_{B_{u,n}}^P(\mathbf{X}_{n-1})}(x|X_{B_{u,n}}^P, \mathbf{X}_{n-1}). \end{aligned}$$

Thus (S24) becomes

$$\begin{aligned} & \mathbb{E}_g \left[\int f_{Y_{u,n}|X_{u,n}}(y_{u,n}^* | x) g_{X_{u,n}^P|X_{B_{u,n}}^P(\mathbf{X}_{n-1})}(x|X_{B_{u,n}}^P, \mathbf{X}_{n-1}) dx \cdot f_{Y_{B_{u,n}}|X_{B_{u,n}}}(y_{B_{u,n}}^* | X_{B_{u,n}}^P) \right] \\ &= \mathbb{E}_g \left[\mathbb{E}_g \left[f_{Y_{u,n}|X_{u,n}}(y_{u,n}^* | X_{u,n}^P) | X_{B_{u,n}}^P, \mathbf{X}_{n-1} \right] \cdot f_{Y_{B_{u,n}}|X_{B_{u,n}}}(y_{B_{u,n}}^* | X_{B_{u,n}}^P) \right] \\ &= \mathbb{E}_g \left[f_{Y_{B_{u,n}^+}|X_{B_{u,n}^+}}(y_{B_{u,n}^+}^* | X_{B_{u,n}^+}^P) \right] \\ &= \mathbb{E}_g \gamma_{B_{u,n}^+}. \end{aligned}$$

Applying the same argument for the special case of $B_{u,n} = A_{u,n}$, we substitute into Assumption B1 to complete the proof with the fact that $h < Q$. \square

Assumption B4. We use subscripts of g to denote marginal and conditional densities derived from (S21). Suppose there is an ϵ_{B4} , independent of U and N , such that the following holds. For each u and n , a set $C_{u,n} \subset (1:U) \times (0:N)$ exists such that $(\tilde{u}, \tilde{n}) \notin C_{u,n}$ implies $B_{u,n}^+ \cap B_{\tilde{u},\tilde{n}}^+ = \emptyset$ and

$$\begin{aligned} & \left| g_{X_{B_{\tilde{u},\tilde{n}} \cup B_{u,n}}^P} - g_{X_{B_{\tilde{u},\tilde{n}}}^P} g_{X_{B_{u,n}}^P} \right| < (1/2) \epsilon_{B4} g_{X_{B_{\tilde{u},\tilde{n}} \cup B_{u,n}}^P} \\ & \left| g_{X_{B_{\tilde{u},\tilde{n}} | \mathbf{X}_{0:N}}^P} g_{X_{B_{u,n} | \mathbf{X}_{0:N}}^P} - g_{X_{B_{\tilde{u},\tilde{n}} \cup B_{u,n} | \mathbf{X}_{0:N}}^P} \right| \\ & < (1/2) \epsilon_{B4} g_{X_{B_{\tilde{u},\tilde{n}} \cup B_{u,n} | \mathbf{X}_{0:N}}^P} \end{aligned}$$

Further, there is a uniform bound $|C_{u,n}| \leq c$.

The mixing of the adapted process in Assumption B4 replaces the mixing of the unconditional process in Assumption A4. Though mixing of the adapted process may be hard to check, one may suspect that the adapted process typically mixes more rapidly than the unconditional process. Assumption B4 is needed only to ensure that the variance bound in Theorem 2 is essentially $O(UN)$ rather than $O(U^2N^2)$. Either of these rates avoids the exponentially increasing variance characterizing the curse of dimensionality. Lower variance than $O(UN)$ cannot be anticipated for any sequential Monte Carlo method since the log likelihood estimate can be written as a sum of UN terms each of which involves its own sequential Monte Carlo calculation. The following Proposition S3 gives an implication of Assumption B4.

Proposition S3. Assumption B4 implies that, if $(\tilde{u}, \tilde{n}) \notin C_{u,n}$,

$$\text{Cov}_g(\gamma_{B_{u,n}}, \gamma_{B_{\tilde{u},\tilde{n}}}) < \epsilon_{B4} Q^{|B_{u,n}|+|B_{\tilde{u},\tilde{n}}|}. \quad (\text{S25})$$

Proof. Write $\gamma = \gamma_{B_{u,n}}$ and $\tilde{\gamma} = \gamma_{B_{\tilde{u},\tilde{n}}}$. Also, write $B = B_{u,n}$, $\tilde{B} = B_{\tilde{u},\tilde{n}}$ and $f_B(x_B^P) = f_{Y_B|X_B}(y_B^* | x_B^P)$. Then,

$$\begin{aligned} \mathbb{E}[\gamma\tilde{\gamma}] &= \int \left[\int f_B(x_B^P) g_{X_B^P | \mathbf{X}_{0:N}}(x_B^P | \mathbf{x}_{0:N}) dx_B^P \right] \\ & \quad \times \left[\int f_{\tilde{B}}(x_{\tilde{B}}^P) g_{X_{\tilde{B}}^P | \mathbf{X}_{0:N}}(x_{\tilde{B}}^P | \mathbf{x}_{0:N}) dx_{\tilde{B}}^P \right] g_{\mathbf{X}_{0:N}}(\mathbf{x}_{0:N}) d\mathbf{x}_{0:N} \\ &= \int \int f_B(x_B^P) f_{\tilde{B}}(x_{\tilde{B}}^P) \left\{ \int g_{X_B^P | \mathbf{X}_{0:N}}(x_B^P | \mathbf{x}_{0:N}) \right. \\ & \quad \left. \times g_{X_{\tilde{B}}^P | \mathbf{X}_{0:N}}(x_{\tilde{B}}^P | \mathbf{x}_{0:N}) g_{\mathbf{X}_{0:N}}(\mathbf{x}_{0:N}) d\mathbf{x}_{0:N} \right\} dx_B^P dx_{\tilde{B}}^P \end{aligned} \quad (\text{S26})$$

Putting the approximate conditional independence requirement of Assumption B4 into (S26), we have

$$\begin{aligned} & \left| \mathbb{E}[\gamma\tilde{\gamma}] - \int f_B(x_B^P) f_{\tilde{B}}(x_{\tilde{B}}^P) g_{X_B^P X_{\tilde{B}}^P | \mathbf{X}_{0:N}}(x_B^P, x_{\tilde{B}}^P | \mathbf{x}_{0:N}) g_{\mathbf{X}_{0:N}}(\mathbf{x}_{0:N}) dx_B^P dx_{\tilde{B}}^P d\mathbf{x}_{0:N} \right| \\ & < (1/2) \epsilon_{B4} Q^{|B|+|\tilde{B}|}. \end{aligned}$$

This gives

$$\left| \mathbb{E}[\gamma\tilde{\gamma}] - \int f_B(x_B^P) f_{\tilde{B}}(x_{\tilde{B}}^P) g_{X_B^P X_{\tilde{B}}^P}(x_B^P, x_{\tilde{B}}^P) dx_B^P dx_{\tilde{B}}^P \right| < (1/2) \epsilon_{B4} Q^{|B|+|\tilde{B}|}. \quad (\text{S27})$$

Then, using the approximate unconditional independence requirement of Assumption B4 combined with the triangle inequality, (S27) implies

$$\left| \mathbb{E}[\gamma\tilde{\gamma}] - \int f_B(x_B^P) f_{\tilde{B}}(x_{\tilde{B}}^P) g_{X_B^P}(x_B^P) g_{X_{\tilde{B}}^P}(x_{\tilde{B}}^P) dx_B^P dx_{\tilde{B}}^P \right| < \epsilon_{B4} Q^{|B|+|\tilde{B}|}. \quad (\text{S28})$$

We can rewrite (S28) as

$$\left| \mathbb{E}[\gamma\tilde{\gamma}] - \mathbb{E}[\gamma] \mathbb{E}[\tilde{\gamma}] \right| < \epsilon_{B4} Q^{|B|+|\tilde{B}|}, \quad (\text{S29})$$

proving the proposition. \square

Assumption B5. *There is a constant K , independent of U and N , such that, for any $0 \leq d \leq d_{\max}$, any $n \geq K + d$, and any set $D \subset (1:U) \times (n:n-d)$,*

$$\begin{aligned} & \left| g_{X_D | \mathbf{X}_{n-d-K}}(x_D | \mathbf{x}_{n-d-K}^{(1)}) - g_{X_D | \mathbf{X}_{n-d-K}}(x_D | \mathbf{x}_{n-d-K}^{(2)}) \right| \\ & < \epsilon_{B5} g_{X_D | \mathbf{X}_{n-d-K}}(x_D | \mathbf{x}_{n-d-K}^{(1)}) \end{aligned}$$

holds for all $\mathbf{x}_{n-d-K}^{(1)}$, $\mathbf{x}_{n-d-K}^{(2)}$, and x_D .

Assumption B5 is needed to ensure the stability of the Monte Carlo approximation to the adapted process. It ensures that any error due to finite Monte Carlo sample size has limited consequences at sufficiently remote time points. One could instead propose a bound that decreases exponentially with K , but that is not needed for the current purposes. The following Proposition S4 is useful for taking advantage of Assumption B5.

Proposition S4. *Suppose that f is a non-negative function and that for some $\epsilon > 0$,*

$$|f(x) - f(x')| < \epsilon f(x')$$

holds for all x, x' . Then for any two probability distributions where the expectations are denoted by \mathbb{E}_1 and \mathbb{E}_2 and for any random variable X , we have

$$|\mathbb{E}_1 f(X) - \mathbb{E}_2 f(X)| \leq \epsilon \mathbb{E}_2 f(X).$$

Proof. Let the two probability laws be denoted by P_1 and P_2 . We have

$$\begin{aligned} |\mathbb{E}_1 f(X) - \mathbb{E}_2 f(X)| &= \left| \int f(x) P_1(dx) - \int f(x') P_2(dx') \right| \\ &\leq \left| \int \int f(x) P_1(dx) P_2(dx') - \int \int f(x') P_1(dx) P_2(dx') \right| \\ &\leq \int \int |f(x) - f(x')| P_1(dx) P_2(dx') \\ &\leq \int \epsilon f(x') P_2(dx') = \epsilon \mathbb{E}_2 f(X). \end{aligned}$$

\square

Assumption B6. Let h be a bounded function with $|h(x)| \leq 1$. Let $\mathbf{X}_{n,S,j,i}^{\text{IR}}$ be the Monte Carlo quantity constructed in ABF-IR, conditional on $\mathbf{X}_{n-1,S,i}^{\text{A}} = \mathbf{x}_{n-1,S,i}^{\text{A}}$. There is a constant $C_0(U, N, S)$ such that, for all $\epsilon_{\text{B6}} > 0$ and $\mathbf{x}_{n-1,S,i}^{\text{A}}$, whenever the number of particles satisfies $J > C_0(U, N, S)/\epsilon_{\text{B6}}^3$,

$$\left| \mathbb{E} \left[\frac{1}{J} \sum_{j=1}^J h(\mathbf{X}_{n,S,j,i}^{\text{IR}}) \right] - \mathbb{E}_g[h(\mathbf{X}_n) \mid \mathbf{X}_{n-1} = \mathbf{x}_{n-1,S,i}^{\text{A}}] \right| < \epsilon_{\text{B6}}.$$

Assumption B6 controls the Monte Carlo error for a single time interval on a single bootstrap replicate. In the case $S = 1$, ABF-IR becomes ABF and this assumption is one of many alternatives for bounding error from importance sampling. The purpose behind the selection of Assumption B6 is to draw on the results of Park and Ionides (2020) for intermediate resampling, and our assumption is a restatement of their Theorem 2. When $S = 1$, the curse of dimensionality for importance sampling has the consequence that C_0 grows exponentially with U . However, Park and Ionides (2020) showed that setting $S = U$ can lead to situations where $C_0(U, N, S)$ in Assumption B6 grows polynomially with U . Here, we do not place requirements concerning the dependence of C_0 on U , N and S since our immediate concern is a limit where \mathcal{I} and J increase. Nevertheless, the numerical results are consistent with the theoretical and empirical results obtained for intermediate resampling in the context of particle filtering by Park and Ionides (2020).

Assumption B7. For $1 \leq n \leq N$, the Monte Carlo random variable $X_{n,i}^{\text{A}}$ is independent of $w_{u,n,i,j}^M$ conditional on $X_{n-1,i}^{\text{A}}$.

The Monte Carlo conditional independence required by Assumption B7 would hold for ABF-IR if the guide variance $V_{u,n,i}$ were calculated using an independent set of guide simulations to those used for evaluating the measurement weights $w_{u,n,i,j}^M$. For numerical efficiency, the ABF-IR algorithm implemented here constructs a shared pool of simulations for both purposes rather than splitting the pool up between them, in the expectation that the resulting minor violation of Assumption B7 has negligible impact.

Theorem 2. Let ℓ^{MC} denote the Monte Carlo likelihood approximation constructed by ABF-IR, or by ABF since this is the special case of ABF-IR with $S = 1$. Consider a limit with a growing number of bootstrap replicates, $\mathcal{I} \rightarrow \infty$, and suppose assumptions B1, B2, B3, B5, B6 and B7. Suppose the number of particles J exceeds the requirement for B6. There are quantities $\epsilon(U, N)$ and $V(U, N)$ with $|\epsilon| < Q^2 \epsilon_{\text{B1}} + 2Q^{2b}(\epsilon_{\text{B5}} + (K + d_{\text{max}})\epsilon_{\text{B6}})$ and $V < Q^{4b}U^2N^2$ such that

$$\mathcal{I}^{1/2}[\ell^{\text{MC}} - \ell - \epsilon UN] \xrightarrow[\mathcal{I} \rightarrow \infty]{d} \mathcal{N}[0, V]. \quad (\text{S30})$$

If additionally Assumption B4 holds, we obtain an improved rate of

$$V < Q^{4b}NU \{c + (\epsilon_{\text{B4}} + 3\epsilon_{\text{B5}} + 4(K + d_{\text{max}})\epsilon_{\text{B6}})(NU - c)\} \quad (\text{S31})$$

Proof. First, we set up some notation. For $B_{u,n}$ and $w_{u,n,i,j}^M$ constructed by ABF-IR, define

$$\gamma_{B_{u,n}}^{\text{MC},i} = \prod_{m=1}^n \left[\frac{1}{J} \sum_{j=1}^J \prod_{(\tilde{u},m) \in B_{\tilde{u},n}^{[m]}} w_{\tilde{u},m,i,j}^M \right] \quad \text{and} \quad \bar{\gamma}_{B_{u,n}}^{\text{MC}} = \frac{1}{\mathcal{I}} \sum_{i=1}^{\mathcal{I}} \gamma_{B_{u,n}}^{\text{MC},i}. \quad (\text{S32})$$

The Monte Carlo conditional likelihoods output by ABF-IR can be written as

$$\ell_{u,n}^{\text{MC}} = \log \bar{\gamma}_{B_{u,n}^+}^{\text{MC}} - \log \bar{\gamma}_{B_{u,n}}^{\text{MC}}. \quad (\text{S33})$$

We proceed with a similar argument to the proof of Theorem 1. Since $\gamma_{B_{u,n}}^{\text{MC},i}$ are i.i.d. for $i \in 1:\mathcal{I}$, we can suppose they are replicates of a Monte Carlo random variable $\gamma_{B_{u,n}}^{\text{MC}}$. We define

$$\Delta_{u,n}^+ = \frac{1}{\sqrt{\mathcal{I}}} \sum_{i=1}^{\mathcal{I}} (\gamma_{B_{u,n}^+}^{\text{MC},i} - \mathbb{E}[\gamma_{B_{u,n}^+}^{\text{MC}}]), \quad \Delta_{u,n} = \frac{1}{\sqrt{\mathcal{I}}} \sum_{i=1}^{\mathcal{I}} (\gamma_{B_{u,n}}^{\text{MC},i} - \mathbb{E}[\gamma_{B_{u,n}}^{\text{MC}}]).$$

The same calculation as (S13) gives

$$\ell_{u,n}^{\text{MC}} = \log \left(\frac{\mathbb{E}[\gamma_{B_{u,n}^+}^{\text{MC}}]}{\mathbb{E}[\gamma_{B_{u,n}}^{\text{MC}}]} \right) + \mathcal{I}^{-1/2} \left(\frac{\Delta_{u,n}^+}{\mathbb{E}[\gamma_{B_{u,n}^+}^{\text{MC}}]} - \frac{\Delta_{u,n}}{\mathbb{E}[\gamma_{B_{u,n}}^{\text{MC}}]} \right) + o_P(\mathcal{I}^{-1/2}) \quad (\text{S34})$$

The joint distribution of $\{(\Delta_{u,n}^+, \Delta_{u,n}), (u, n) \in 1:U \times 1:N\}$ follows a standard central limit theorem as $\mathcal{I} \rightarrow \infty$. Each term has mean zero, with variances and covariances uniformly bounded over $(u, n, \tilde{u}, \tilde{n})$ due to Assumption B3. From Proposition S2, using the same reasoning as (S18),

$$\left| \log \left(\frac{\mathbb{E}_g[\gamma_{A_{u,n}^+}]}{\mathbb{E}_g[\gamma_{A_{u,n}}]} \right) - \log \left(\frac{\mathbb{E}_g[\gamma_{B_{u,n}^+}]}{\mathbb{E}_g[\gamma_{B_{u,n}}]} \right) \right| < \epsilon_{\text{B1}} Q^2. \quad (\text{S35})$$

Now we use Lemma S2 and (S17) to obtain

$$\begin{aligned} & \left| \log \left(\frac{\mathbb{E}_g[\gamma_{B_{u,n}^+}]}{\mathbb{E}_g[\gamma_{B_{u,n}}]} \right) - \log \left(\frac{\mathbb{E}[\gamma_{B_{u,n}^+}^{\text{MC}}]}{\mathbb{E}[\gamma_{B_{u,n}}^{\text{MC}}]} \right) \right| \\ & \leq \left| \log \mathbb{E}_g[\gamma_{B_{u,n}^+}] - \log \mathbb{E}[\gamma_{B_{u,n}^+}^{\text{MC}}] \right| + \left| \log \mathbb{E}_g[\gamma_{B_{u,n}}] - \log \mathbb{E}[\gamma_{B_{u,n}}^{\text{MC}}] \right| \\ & < 2Q^{2b} (\epsilon_{\text{B5}} + (K + d_{\text{max}}) \epsilon_{\text{B6}}). \end{aligned} \quad (\text{S36})$$

The proof of the central limit result in (S30) is completed by combining (S34), (S35) and (S36). To show (S31) we check that $\Delta_{u,n}$ and $\Delta_{\tilde{u},\tilde{n}}$ are weakly correlated when (u, n) and (\tilde{u}, \tilde{n}) are sufficiently separated. By the same reasoning as the proof of Theorem 1, it is sufficient to show that $\gamma_{B_{u,n}}^{\text{MC}}$ and $\gamma_{B_{\tilde{u},\tilde{n}}}^{\text{MC}}$ are weakly correlated. These Monte Carlo quantities approximate $\gamma_{B_{u,n}}(\mathbf{X}_{0:n-1})$ and $\gamma_{B_{\tilde{u},\tilde{n}}}(\mathbf{X}_{0:\tilde{n}-1})$ with \mathbf{X} drawn from g . Let us suppose $n \geq \tilde{n}$, and write $d_{u,n} = n - \inf_{(v,m) \in B_{u,n}} m$. First, we consider the situation $n - \tilde{n} > K + d_{u,n}$, in which case we can use the Markov property to give

$$\text{Cov}(\gamma_{B_{u,n}}^{\text{MC}}, \gamma_{B_{\tilde{u},\tilde{n}}}^{\text{MC}}) < \mathbb{E}[\gamma_{B_{\tilde{u},\tilde{n}}}^{\text{MC}}] \sup_{\mathbf{x}} \left\{ \mathbb{E}[\gamma_{B_{u,n}}^{\text{MC}} | \mathbf{X}_{n-d_{u,n}-K,1}^A = \mathbf{x}] - \mathbb{E}[\gamma_{B_{u,n}}^{\text{MC}}] \right\} \quad (\text{S37})$$

Then, the triangle inequality followed by applications of Assumption B5 and Lemma S2 gives

$$\begin{aligned}
& \left| \mathbb{E}[\gamma_{B_{u,n}}^{MC} | \mathbf{X}_{n-d_{u,n}-K,1}^A = \mathbf{x}] - \mathbb{E}[\gamma_{B_{u,n}}^{MC}] \right| \\
& \leq \left| \mathbb{E}_g[\gamma_{B_{u,n}} | \mathbf{X}_{n-d_{u,n}-K} = \mathbf{x}] - \mathbb{E}_g[\gamma_{B_{u,n}}] \right| \\
& \quad + \left| \mathbb{E}[\gamma_{B_{u,n}}^{MC} | \mathbf{X}_{n-d_{u,n}-K,1}^A = \mathbf{x}] - \mathbb{E}_g[\gamma_{B_{u,n}} | \mathbf{X}_{n-d_{u,n}-K} = \mathbf{x}] \right| \\
& \quad + \left| \mathbb{E}[\gamma_{B_{u,n}}^{MC}] - \mathbb{E}_g[\gamma_{B_{u,n}}] \right| \\
& \leq Q^b \left(2\epsilon_{B5} + 2(K + d_{u,n})\epsilon_{B6} \right)
\end{aligned} \tag{S38}$$

Putting (S38) into (S37), we get

$$\text{Cov}(\gamma_{B_{u,n}}^{MC}, \gamma_{B_{\tilde{u},\tilde{n}}}^{MC}) < Q^{2b} \left(2\epsilon_{B5} + 2(K + d_{u,n})\epsilon_{B6} \right). \tag{S39}$$

Now we address the situation $n - \tilde{n} \leq K + d_{u,n}$. We apply Lemma S2 on the union $B_{u,n} \cup B_{\tilde{u},\tilde{n}}$ for which the temporal depth is bounded by $d \leq K + d_{u,n} + d_{\tilde{u},\tilde{n}}$. This gives

$$\left| \mathbb{E}[\gamma_{B_{u,n}}^{MC} \gamma_{B_{\tilde{u},\tilde{n}}}^{MC}] - \mathbb{E}_g[\gamma_{B_{u,n}} \gamma_{B_{\tilde{u},\tilde{n}}}] \right| < Q^{2b} \left((2K + d_{u,n} + d_{\tilde{u},\tilde{n}})\epsilon_{B6} + \epsilon_{B5} \right). \tag{S40}$$

From Proposition S3, if $(\tilde{u},\tilde{n}) \notin C_{u,n}$,

$$\text{Cov}_g(\gamma_{B_{u,n}}, \gamma_{B_{\tilde{u},\tilde{n}}}) < \epsilon_{B4} Q^{2b}. \tag{S41}$$

Now, we establish that $\text{Cov}(\gamma_{B_{u,n}}^{MC}, \gamma_{B_{\tilde{u},\tilde{n}}}^{MC})$ is close to $\text{Cov}_g(\gamma_{B_{u,n}}, \gamma_{B_{\tilde{u},\tilde{n}}})$.

$$\begin{aligned}
& \left| \text{Cov}(\gamma_{B_{u,n}}^{MC}, \gamma_{B_{\tilde{u},\tilde{n}}}^{MC}) - \text{Cov}_g(\gamma_{B_{u,n}}, \gamma_{B_{\tilde{u},\tilde{n}}}) \right| \\
& \leq \left| \mathbb{E}[\gamma_{B_{u,n}}^{MC} \gamma_{B_{\tilde{u},\tilde{n}}}^{MC}] - \mathbb{E}_g[\gamma_{B_{u,n}} \gamma_{B_{\tilde{u},\tilde{n}}}] \right| \\
& \quad + \left| \mathbb{E}[\gamma_{B_{u,n}}^{MC}] (\mathbb{E}[\gamma_{B_{\tilde{u},\tilde{n}}}^{MC}] - \mathbb{E}_g[\gamma_{B_{\tilde{u},\tilde{n}}})) \right| \\
& \quad + \left| \mathbb{E}[\gamma_{B_{\tilde{u},\tilde{n}}}^{MC}] (\mathbb{E}[\gamma_{B_{u,n}}^{MC}] - \mathbb{E}_g[\gamma_{B_{u,n}}]) \right| \\
& < Q^{2b} \left((2K + d_{u,n} + d_{\tilde{u},\tilde{n}})\epsilon_{B6} + \epsilon_{B5} + 2(\epsilon_{B5} + (K + d_{\max})\epsilon_{B6}) \right). \\
& < Q^{2b} \left(3\epsilon_{B5} + 4(K + d_{\max})\epsilon_{B6} \right)
\end{aligned} \tag{S42}$$

Using (S42) together with (S41) to bound the $UN(UN - c)$ off-diagonal covariance terms completes the derivation of (S31). \square

Lemma S2. *Suppose Assumptions B3, B5, B6 and B7. Suppose the number of particles J exceeds the requirement for B6. If we write $d_B = \max_{(u_1, n_1), (u_2, n_2) \in B} |n_1 - n_2|$ for $B \subset 1:U \times 1:N$, then for any B ,*

$$\left| \mathbb{E}[\gamma_B^{MC} | \mathbf{X}_{n-d_B-K,1}^A = \mathbf{x}] - \mathbb{E}_g[\gamma_B | \mathbf{X}_{n-d_B-K} = \mathbf{x}] \right| < Q^{|B|} (K + d_B)\epsilon_{B6}, \quad \forall \mathbf{x} \in \mathbb{X}^U,$$

and

$$\left| \mathbb{E}[\gamma_B^{MC}] - \mathbb{E}_g[\gamma_B] \right| < Q^{|B|} (\epsilon_{B5} + (K + d_B)\epsilon_{B6}). \tag{S43}$$

Proof. Suppose that $\max_{(u',n') \in B} n' = n$. Define $\eta_m(\mathbf{x}_n) = 1$ and, for $0 \leq m \leq n-1$,

$$\eta_m(\mathbf{x}_m) = \mathbb{E}_g \left[\prod_{k=m+1}^n \gamma_{B^{[k]}} \middle| \mathbf{X}_m = \mathbf{x}_m \right]. \quad (\text{S44})$$

We have a recursive identity

$$\eta_m(\mathbf{X}_m) = \mathbb{E}_g \left[\gamma_{B^{[m+1]}} \eta_{m+1}(\mathbf{X}_{m+1}) \middle| \mathbf{X}_m \right]. \quad (\text{S45})$$

By taking the expectation of (S44), we have

$$\mathbb{E}_g[\eta_0(\mathbf{X}_0)] = \mathbb{E}_g[\gamma_B]. \quad (\text{S46})$$

Note that g has marginal density $f_{\mathbf{X}_0}$ for \mathbf{X}_0 . We analyze an ABF-IR approximation to (S45). The function $\eta_{m+1}(\mathbf{x})$ is not in practice computationally available for evaluation via ABF-IR, but the recursion nevertheless leads to a useful bound. Let $\mathbf{X}_{m+1}^A[j](\mathbf{x}_m)$ correspond to the variable $\mathbf{X}_{m+1, S, 1, j}^{IR}$ constructed by ABF-IR conditional on $\mathbf{X}_{m, 1}^A = \mathbf{x}_m$. Equivalently, $\mathbf{X}_{m+1}^A[j](\mathbf{x}_m)$ matches the variable $\mathbf{X}_{m+1, 1}^A$ in ABF-IR if the assignment $\mathbf{X}_{m+1, 1}^A = \mathbf{X}_{m+1, S, 1, 1}^{IR}$ is replaced by $\mathbf{X}_{m+1, 1}^A = \mathbf{X}_{m+1, S, 1, j}^{IR}$ conditional on $\mathbf{X}_{m, 1}^A = \mathbf{x}_m$. We define an approximation error $e_m(\mathbf{x}_m)$ by

$$\eta_m(\mathbf{x}_m) = \frac{1}{J} \sum_{j=1}^J f_{Y_{B^{[m+1]}} | \mathbf{X}_m}(y_{B^{[m+1]}}^* | \mathbf{x}_m) \eta_{m+1}(\mathbf{X}_{m+1}^A[j](\mathbf{x}_m)) + e_m(\mathbf{x}_m). \quad (\text{S47})$$

From Assumptions B3 and B6, $\mathbb{E}|e_m(\mathbf{x}_m)| < \epsilon_{B6} Q^{|B^{[m+1:n]}|}$ uniformly over \mathbf{x}_m . Thus, setting $r_m = \mathbb{E}|e_m(\mathbf{X}_{m, 1}^A)|$, we have

$$r_m < \epsilon_{B6} Q^{|B^{[m+1:n]}|}. \quad (\text{S48})$$

Now, setting $K' = K + d_{u, n}$, we commence to prove inductively that, for $n - K' \leq m \leq n$,

$$\left| \eta_{m-K'}(\mathbf{x}) - \mathbb{E} \left[\eta_m(\mathbf{X}_{m, 1}^A) \prod_{k=n-K'+1}^m f_{Y_{B^{[k]}} | \mathbf{X}_{k-1}}(y_{B^{[k]}}^* | \mathbf{X}_{k-1, 1}^A) \middle| \mathbf{X}_{n-K', 1}^A = \mathbf{x} \right] \right| < (m-n+K') \epsilon_{B6} Q^{|B|}. \quad (\text{S49})$$

First, suppose that (S49) holds for m . From (S47) and (S48),

$$\left| \eta_m(\mathbf{x}_m) - \mathbb{E} \left[\frac{1}{J} \sum_{j=1}^J f_{Y_{B^{[m+1]}} | \mathbf{X}_m}(y_{B^{[m+1]}}^* | \mathbf{x}_m) \eta_{m+1}(\mathbf{X}_{m+1}^A[j](\mathbf{x}_m)) \right] \right| < \epsilon_{B6} Q^{|B^{[m+1:n]}|}. \quad (\text{S50})$$

Since the particles are exchangeable, the expectation of the mean of J particles can be replaced with the expectation of the first particle. Plugging in $\mathbf{x}_m = \mathbf{X}_{m, 1}^A$ gives us

$$\left| \eta_m(\mathbf{X}_{m, 1}^A) - f_{Y_{B^{[m+1]}} | \mathbf{X}_m}(y_{B^{[m+1]}}^* | \mathbf{X}_{m, 1}^A) \mathbb{E} [\eta_{m+1}(\mathbf{X}_{m+1, 1}^A) | \mathbf{X}_{m, 1}^A] \right| < \epsilon_{B6} Q^{|B^{[m+1:n]}|} \quad (\text{S51})$$

Putting (S51) into (S49), for $m \leq n$, and taking an iterated expectation with respect to $\mathbf{X}_{m, 1}^A$, we find that (S49) holds also for $m+1$. Since (S49) holds trivially for $m = n - K'$, it holds for $n - K' \leq m \leq n$ by induction. Then, noting $\eta_n(\mathbf{x}) = 1$, we have from (S49) that

$$\left| \eta_{m-K'}(\mathbf{x}) - \mathbb{E} \left[\prod_{k=n-K'+1}^n f_{Y_{B^{[k]}} | \mathbf{X}_{k-1}}(y_{B^{[k]}}^* | \mathbf{X}_{k-1, 1}^A) \middle| \mathbf{X}_{n-K', 1}^A = \mathbf{x} \right] \right| < K' \epsilon_{B6} Q^{|B|}.$$

Integrating the above inequality over \mathbf{x} with respect to the law of $\mathbf{X}_{n-K',1}^A$, we obtain

$$\left| \mathbb{E}[\eta_{n-K'}(\mathbf{X}_{n-K',1}^A)] - \mathbb{E} \left[\prod_{k=n-K'+1}^n f_{Y_{B^{[k]}|\mathbf{X}_{k-1}}}(y_{B^{[k]}|}^* | \mathbf{X}_{k-1,1}^A) \right] \right| < K' \epsilon_{B6} Q^{|B|}. \quad (\text{S52})$$

But under Assumption B7, we have

$$\mathbb{E} \left[\prod_{k=n-K'+1}^n f_{Y_{B^{[k]}|\mathbf{X}_{k-1}}}(y_{B^{[k]}|}^* | \mathbf{X}_{k-1,1}^A) \right] = \mathbb{E}[\gamma_B^{MC}]. \quad (\text{S53})$$

Assumption B5 says

$$|\eta_{n-K'}(\mathbf{x}_{n-K'}^{(1)}) - \eta_{n-K'}(\mathbf{x}_{n-K'}^{(2)})| < \epsilon_{B5} \eta_{n-K'}(\mathbf{x}_{n-K'}^{(2)}). \quad (\text{S54})$$

Application of Proposition S4 to (S54) gives

$$\left| \mathbb{E}_g[\eta_{n-K'}(\mathbf{X}_{n-K'})] - \mathbb{E}[\eta_{n-K'}(\mathbf{X}_{n-K',1}^A)] \right| < \epsilon_{B5} \mathbb{E}_g[\eta_{n-K'}(\mathbf{X}_{n-K'})] < \epsilon_{B5} Q^{|B|}. \quad (\text{S55})$$

Combining (S52), (S53), and (S55) completes the proof of Lemma S2. \square

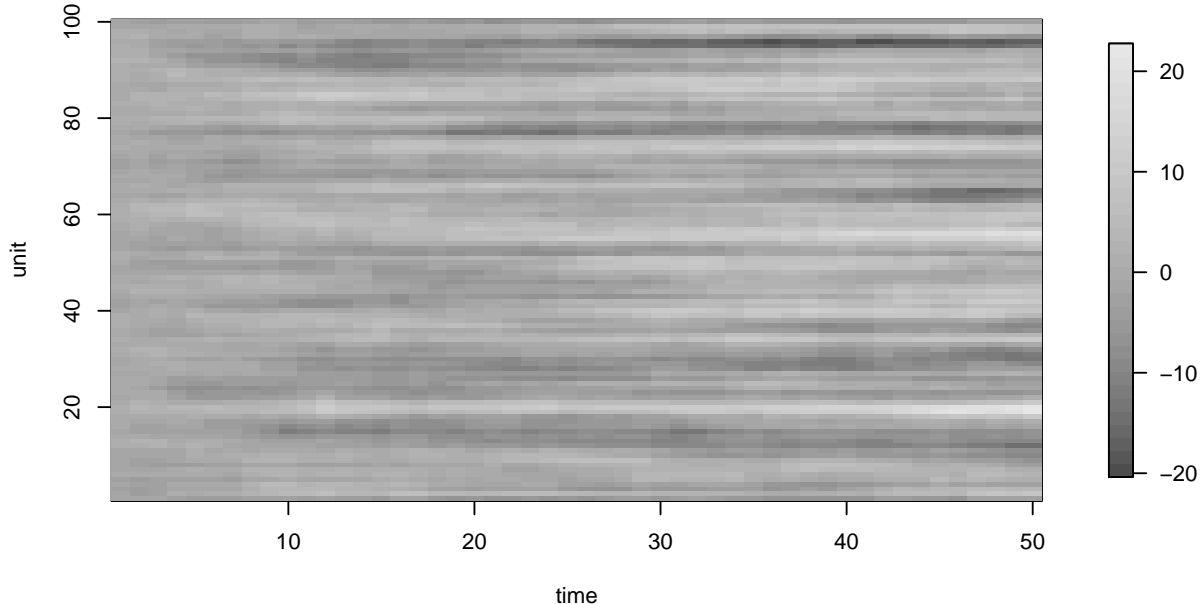


Figure S-1: correlated Brownian motion simulation used in the main text

S5 The correlated Brownian motion example

To help visualize the correlated Brownian motion model, Fig. S-1 shows one of the simulations used for the results in Figure 4 of the main text. Table S-1 gives the algorithmic settings used for the filters and corresponding computational resource requirements. Broadly speaking, \mathcal{IJ} for ABF and AIRSIF should be compared with \mathcal{I} for UBF, J for PF, and JG for GIRF.

The computational effort allocated to each algorithm in Table S-1 is given in core minutes. UBF, ABF and ABF-IR parallelize readily, which is less true for PF and GIRF. Therefore, the UBF, ABF and ABF-IR implementations run on all available cores (36 for this experiment) whereas the PF and GIRF implementations run on a single core. If sufficient replications are being carried out to utilize all available cores, comparison of core minute utilization is equivalent to comparison of total computation time. However, a single replication of UBF, ABF or ABF-IR proceeds more quickly due to the parallelization.

ABF-IR and GIRF have computational time scaling quadratically with U in this example, whereas the other methods scale linearly. This is because the number of intermediate steps used, S , grows linearly with U .

The main purpose of this example is not to provide a comparison between the functional capabilities of the methods on interesting scientific problems. It is a toy example without the complexities that the methods are intended to address. This simple example does show clearly the quick decline of PF and the slower declines of GIRF and ABF as dimension increases.

	UBF	ABF	ABF-IR	GIRF	PF	BPF	EnKF
particles, J	—	400	200	1000	100000	20000	10000
bootstrap replications, \mathcal{I}	40000	400	200	—	—	—	—
guide simulations, G	—	—	—	50	—	—	—
lookahead lag, L	—	—	—	2	—	—	—
intermediate steps, S	—	—	$U/2$	U	—	—	—
neighborhood, $B_{u,n}$ or block size	$\{(u-1,n),(u-2,n),$ $(u,n-1),(u,n-2)\}$			—	—	3	—
forecast mean, $\boldsymbol{\mu}(\boldsymbol{x}, s, t)$	—	—	\boldsymbol{x}		—	—	—
measurement mean, $h_{u,n}(x)$	—	—	x		—	—	x
$\tau = \overleftarrow{v}_{u,n}(V, x)$	—	—	\sqrt{V}		—	—	—
$V = \overrightarrow{v}_{u,n}(\tau, x)$	—	—	τ^2		—	—	τ^2
effort (core mins, $U = 100$)	0.9	2.1	4.2	0.3	0.3	0.2	0.0
effort (core mins, $U = 80$)	1.4	3.2	12.1	0.7	0.6	0.3	0.1
effort (core mins, $U = 60$)	2.2	6.0	32.0	1.9	1.3	0.6	0.2
effort (core mins, $U = 30$)	4.0	11.6	87.1	6.1	3.2	1.3	0.4
effort (core mins, $U = 10$)	7.6	26.1	311.6	47.1	9.1	3.2	1.1

Table S-1: Algorithmic settings for the correlated Brownian motion numerical example. Computational effort is measured in core minutes for running one filter, corresponding to a point on Figure 1 in the main text. The time taken for computing a single point using the parallel UBF, ABF and ABF-IR implementations is the effort divided by the number of cores, here 40. The time taken for computing a single point using the single-core GIRF, PF, BPF and EnKF implementations is equal to the effort in core minutes.

parameter	value	unit	description
$\bar{\beta}$	1560.6	year ⁻¹	mean contact rate
$\mu_{\bullet D}^{-1}$	50.0	year	mean duration in the population
μ_{EI}^{-1}	7.0	day	latent period
μ_{IR}^{-1}	7.0	day	infectious period
σ_{SE}	0.150	year ^{1/2}	process noise
a	0.500	—	amplitude of seasonality
α	1	—	mixing exponent
τ	4	year	delay from birth to entry into susceptibles
ρ	0.5	—	reporting probability
ψ	0.15	—	reporting overdispersion
G	400	—	gravitation constant
$S_u(0), u \in 1 : U$	0.032	—	initial susceptible fraction
$E_u(0), u \in 1 : U$	0.00005	—	initial exposed fraction
$I_u(0), u \in 1 : U$	0.00004	—	initial infectious fraction

Table S-2: Parameters for the spatiotemporal measles transmission model

S6 The measles example

Table S-2 gives the model parameter values and Table S-3 gives the algorithmic settings used for the filters. The times in Table S-3 give the total time required by each algorithm to calculate all its results for Figure 3 in the main text, using 36 cores. The expected forecast function $\mu(x, s, t)$ needed for ABF-IR and GIRF was computed using a numerical solution to the deterministic skeleton of the stochastic model, i.e, a system of ODEs with derivative matching the infinitesimal mean function of the stochastic dynamic model. In the specifications of $h_u(x)$, $\bar{v}_u(V, x, \theta)$ and $\vec{v}_u(\theta, x)$, the latent process value x contains a variable C giving the cumulative removed infections in the current observation interval.

In Table S-3, we see that the effort allocated to UBF, ABF and PF scales linearly with U , since the number of bootstrap replications and particles is fixed in this experiment. GIRF computational effort scales fairly linearly in U , since its effort is dominated by the guide simulations (which are linear in U) rather than by the intermediate timestep calculations (which are quadratic in U since we carry out U intermediate calculations each of size linear in U). The effort allocated to ABF-IR scales with U^2 , since ABF-IR is more parsimonious with guide simulations (all particles in one bootstrap replication share the same guide simulations) and so the intermediate timestep calculations dominate the effort. To obtain stable variance in the log likelihood estimate, the number of particles and bootstrap replications would have to grow with U . However, given a constraint on total computational resources, the number of particles and bootstrap replications would have to shrink as U increases. The limit studied in this experiment is a balance between the two: the assumption is that one is prepared to invest a growing amount of computational effort as the data grow, but this should not grow too fast. ABF-IR was permitted the greatest computational effort, but the following two considerations balance this:

	UBF	ABF	ABF-IR	GIRF	EnKF	PF	BPF
particles, J	1	500	200	2000	10000	100000	20000
replicates, \mathcal{I}	20000	500	200	—	—	—	—
guide simulations, G	—	—	—	40	—	—	—
lookahead lag, L	—	—	—	1	—	—	—
intermediate steps, S	—	—	$U/2$	U	—	—	—
neighborhood, $B_{u,n}$ or block size	$\{(u, n - 1), (u, n - 2)\}$			—	—	—	2
measurement mean, $h_{u,n}(x)$	—	—	ρC		—	—	—
$V = \vec{v}_{u,n}(\psi, \rho, x)$	—	—	$\rho(1 - \rho)C + \rho^2 C^2 \psi^2$		—	—	—
forecast mean, $\boldsymbol{\mu}(\mathbf{x}, s, t)$	—	—	ODE model		—	—	—
$\psi = \overleftarrow{v}_{u,n}(V, x)$	—	—	$\frac{\sqrt{V - \rho(1 - \rho)C}}{\rho C}$		—	—	—
effort (core mins, $U = 2$)	28.4	11.5	6.4	2.6	0.3	3.2	0.8
effort (core mins, $U = 4$)	35.7	19.0	19.0	5.5	0.6	5.9	1.5
effort (core mins, $U = 8$)	52.5	35.0	60.1	12.7	1.2	11.5	2.9
effort (core mins, $U = 16$)	87.9	66.7	217.8	36.3	2.4	22.5	5.8
effort (core mins, $U = 32$)	155.2	133.3	1032.1	133.7	4.7	45.3	11.6

Table S-3: Algorithmic settings for the measles example calculations in Figures 3 and 4. Computational effort is measured in core minutes for running one filter, corresponding to a point on Figure 3. The time taken for computing a single point using the parallel UBF, ABF and ABF-IR implementations is the effort divided by the number of cores, here 36. The time taken for computing a single point using the single core GIRF, EnKF, PF and BPF implementations is equal to the effort in core minutes.

1. Parallelization. UBF, ABF and ABF-IR are trivially parallelizable. The value of parallelization depends, among other things, on how many replications are being computed simultaneously and on how many cores are available. Nevertheless, it is helpful that the core minute effort requirement for ABF and ABF-IR can be divided by the number of available cores to give the computational time. Parallelizations of GIRF and PF can be constructed (Park and Ionides, 2020) but these involve non-trivial interaction between processors leading to additional algorithmic complexity and computational overhead.
2. Memory. The intermediate timestep calculations in ABF-IR and GIRF do not add to the memory requirement, and the memory demands of UBF, ABF and ABF-IR are distributed across the parallel computations. A basic PF implementation for a large model can become constrained by its memory requirement (linear in the number of particles) before it can match the processor effort employed by the other algorithms.

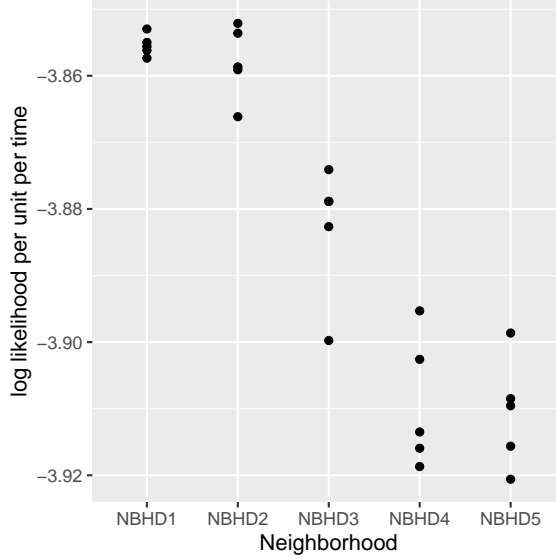


Figure S-2: log likelihood estimates for simulated data from the measles model using ABF, with varying neighborhoods.

S7 Varying the neighborhood for measles

We compared five different neighborhoods for the measles model:

NBHD1	One co-located lag	$\{(u, n - 1)\}$
NBHD2	Two co-located lags	$\{(u, n - 1), (u, n - 2)\}$
NBHD3	Three co-located lags	$\{(u, n - 1), (u, n - 2), (u, n - 3)\}$
NBHD4	Two co-located lags and the previous city	$\{(u, n - 1), (u, n - 2), (u - 1, n)\}$
NBHD5	Two co-located lags and London	$\{(u, n - 1), (u, n - 2), (1, n)\}$

We filtered simulated data for $U = 40$ and $N = 130$, with 10 replications. We used ABF with 200 particles on each of 1000 bootstrap replications. The results are shown in Fig. S-2. Larger neighborhoods should increase the expected likelihood, but their increased Monte Carlo variability can decrease the expected log likelihood due to Jensen’s inequality. In this case, we see that a neighborhood of two co-located lags provides a reasonable bias-variance tradeoff. The time taken for the above calculation was insensitive to the size of the neighborhood. The total run time for each neighborhood in Fig. S-2 was 223.0 mins for NBHD1, 225.5 mins for NBHD2, 225.4 mins for NBHD3, 218.6 mins for NBHD4, 234.8 mins for NBHD5.

S8 A Lorenz-96 example

Our primary motivation for ABF and ABF-IR is application to population dynamics arising in ecological and epidemiological models. Geophysical models provide an alternative situation involving spatiotemporal data analysis. We compare methods on the Lorenz-96 model, a nonlinear chaotic system providing a toy model for global atmospheric circulation (Lorenz, 1996; van Kekem and Sterk, 2018). We consider a stochastic Lorenz-96 model with added Gaussian process noise (Park and Ionides, 2020) defined as the solution to the following system of stochastic differential equations,

$$dX_u(t) = \{(X_{u+1}(t) - X_{u-2}(t)) \cdot X_{u-1}(t) - X_u(t) + F\}dt + \sigma_p dB_u(t), \quad u \in 1:U. \quad (\text{S56})$$

We define $X_0 = X_U$, $X_{-1} = X_{U-1}$, and $X_{U+1} = X_1$ so that the U spatial locations are placed on a circle. The terms $\{B_u(t), u \in 1:U\}$ denote U independent standard Brownian motions. F is a forcing constant, and we use the value $F = 8$ which was demonstrated by Lorenz (1996) to induce chaotic behavior. The process noise parameter is set to $\sigma_p = 1$. The system is started with initial state $X_u(0)$ drawn as an independent normal random variable with mean 5 and standard deviation 2 for $u \in 1:U$. This initialization leads to short transient behavior. Observations are independently made for each dimension at $t_n = n$ for $n \in 1:N$ with Gaussian measurement noise of mean zero and standard deviation $\tau = 1$,

$$Y_{u,n} = X_u(t_n) + \eta_{u,n} \quad \eta_{u,n} \sim N(0, \tau^2). \quad (\text{S57})$$

We used an Euler-Maruyama method for numerical approximation of the sample paths of $\{\mathbf{X}(t)\}$, with timestep of 0.005. A simulation from this model is shown in Fig. S-4.

The ensemble Kalman filter (EnKF) is a widely used filtering method in weather forecasting for high dimensional systems (Evensen and van Leeuwen, 1996). EnKF involves a local Gaussian approximation which is problematic in highly nonlinear systems (Ades and Van Leeuwen, 2015). Methods that make local Gaussian assumptions like EnKF are necessary to scale up to the dimensions of the problems in weather forecasting. Figure S-3 shows that for a small number of units, the basic particle filter (PF) and GIRF out-perform EnKF. Then, as the number of spatial units increases, the performance of PF rapidly deteriorates whereas GIRF continues to perform well up to a moderate number of units. UBF, ABF, and particularly ABF-IR, scales well despite underperforming EnKF on this example. The additive Gaussian observation and process noise in the Lorenz-96 model is well suited to the approximations involved in EnKF. By contrast, it is less clear how to apply EnKF to discrete population non-Gaussian models such as the measles example, and how effective the resulting approximations might be.

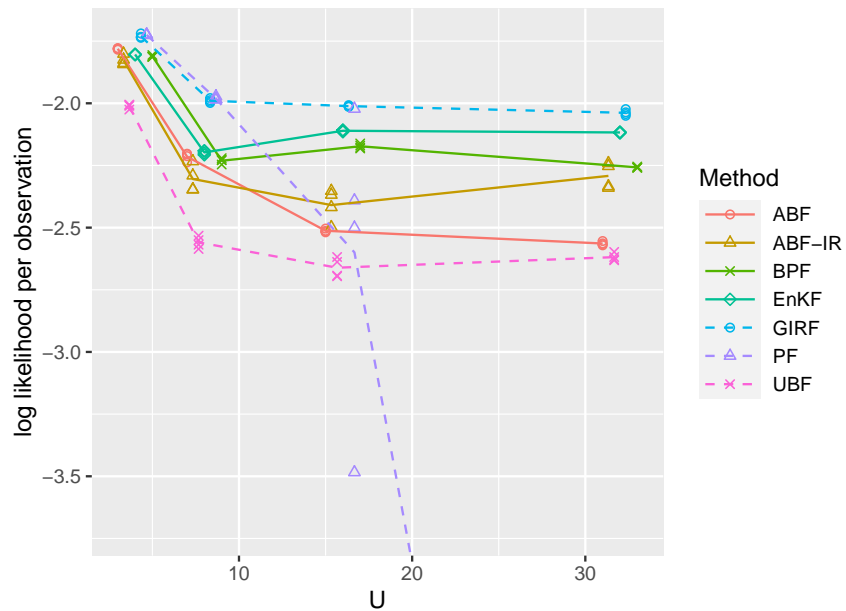


Figure S-3: Log likelihood estimates for a Lorenz-96 model of various dimensions. UBF, ABF and ABF-IR are compared with a guided intermediate resampling filter (GIRF), a standard particle filter (PF), a block particle filter (BPF) and an ensemble Kalman filter (EnKF).

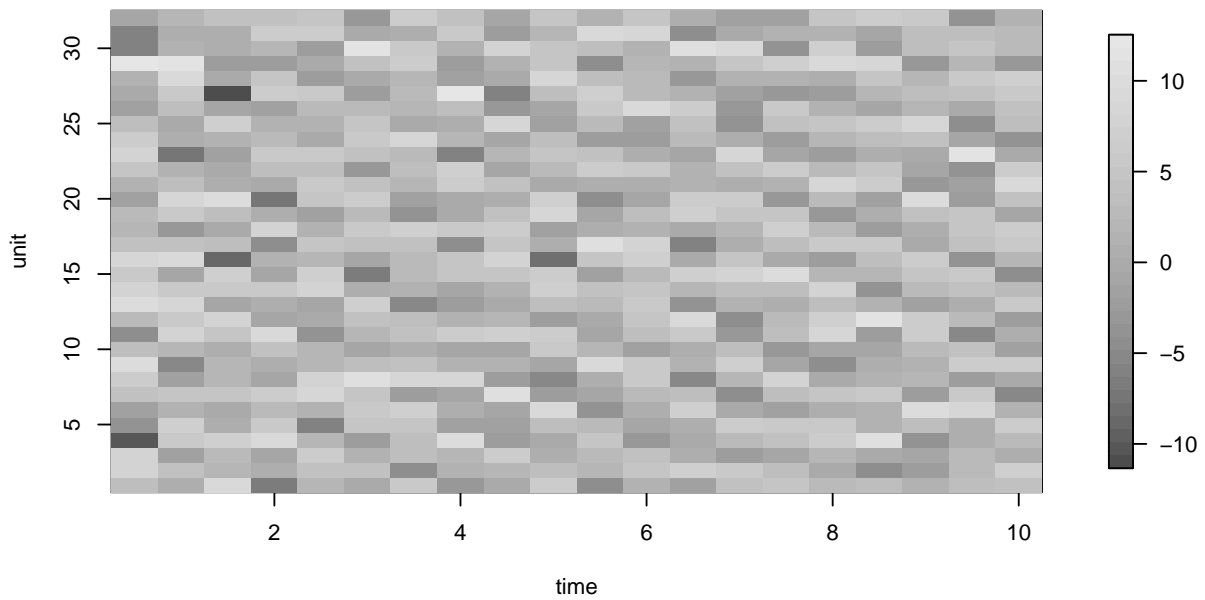


Figure S-4: Lorenz '96 simulation used in the main text

	UBF	ABF	ABF-IR	GIRF	PF	EnKF	BPF
particles, J	1	400	200	1000	100000	10000	10000
bootstrap replicates, \mathcal{I}	40000	400	200	—	—	—	—
guide simulations, G	—	—	—	50	—	—	—
lookahead lag, L	—	—	—	2	—	—	—
intermediate steps, S	—	—	$U/2$	U	—	—	—
neighborhood, $B_{u,n}$ or block size	$\{(u,n-1),(u,n-2),$ $(u-1,n),(u-2,n)\}$			—	—	—	4
forecast mean, $\boldsymbol{\mu}(\boldsymbol{x}, s, t)$	—	—	ODE model		—	—	—
measurement mean, $h_{u,n}(x)$	—	—	x		—	x	—
$\tau = \overleftarrow{v}_{u,n}(V, x)$	—	—	\sqrt{V}		—	—	—
$V = \overrightarrow{v}_{u,n}(\tau, x)$	—	—	τ^2		—	τ^2	—
effort (core mins, $U = 4$)	34.5	5.2	5.1	2.0	2.0	0.2	0.2
effort (core mins, $U = 6$)	40.9	7.3	8.2	3.0	2.9	0.3	0.3
effort (core mins, $U = 10$)	54.5	11.2	16.3	5.0	4.8	0.5	0.5
effort (core mins, $U = 16$)	75.5	16.8	33.7	8.3	7.6	0.8	0.9
effort (core mins, $U = 50$)	202.3	48.6	174.8	34.4	23.7	2.5	2.7

Table S-4: Algorithmic settings for the Lorenz-96 numerical example. Computational effort is measured in core minutes for running one filter, corresponding to a point on Figure Figure S-3. The time taken for computing a single point using the parallel UBF, ABF and ABF-IR implementations is the effort divided by the number of cores, here 36. The time taken for computing a single point using the single-core GIRF, PF, EnKF and BPF implementations is equal to the effort in core minutes.

S9 A memory-efficient representation of ABF

The ABF pseudocode in the main text emphasizes the logical structure of the mathematical quantities computed, rather than describing a specific implementation. Arguably, an algorithm should specify not only what is to be computed, but also details of what variables should be created and saved to carry out these computations efficiently, and how computations and storage are shared across multiple locations when the algorithm is parallelized. We use the term algorithm to denote a higher level description of the quantities to be calculated and we will say that alternative pseudocodes arriving at the same quantities are representations of the algorithm. Here, we present an alternative representations of ABF which we call ABF₂, and we refer to the representation in the main text as ABF₁. The most concrete form of an algorithm is the actual computer code implementing the algorithm in a programming language. The implementation of ABF in `spatPomp`, used for numerical results in this paper, uses an embarrassingly parallel approach based on the representation ABF₁. This strategy facilitates robust and simple parallelization, and is appropriate when memory constraints are not limiting. To develop ABF₂, we set up notation similar to that used for the mathematical theory. Let

$$\gamma_{u,n,i,k} = \frac{1}{J} \sum_{j=1}^J \prod_{\tilde{u}: (\tilde{u}, n-k) \in B_{u,n}} w_{\tilde{u}, n-k, i, j}^M \quad (\text{S58})$$

Also, let

$$\gamma_{u,n,i,0}^+ = \frac{1}{J} \sum_{j=1}^J \prod_{(\tilde{u}, n) \in B_{u,n}^+} w_{\tilde{u}, n, i, j}^M \quad (\text{S59})$$

Now set K to be the largest value of k for which $B_{u,n}^{[n-k]}$ is nontrivial for some (u, n) , i.e., K is the largest temporal lag in any neighborhood. With this notation, we can write (S32) as

$$\begin{aligned} \gamma_{B_{u,n}}^{MC,i} &= \prod_{k=0}^K \gamma_{u,n,i,k} \\ \gamma_{B_{u,n}^+}^{MC,i} &= \gamma_{u,n,i,0}^+ \prod_{k=1}^K \gamma_{u,n,i,k} \end{aligned}$$

This motivates the following representation of ABF.

ABF₂. Adapted bagged filter, representation 2.

Initialize adapted simulation: $\mathbf{X}_{0,i}^A \sim f_{\mathbf{X}_0}(\mathbf{x}_0)$

For n in $1:N$

Proposals: $\mathbf{X}_{n,i,j}^P \sim f_{\mathbf{X}_n|X_{1:U,n-1}}(\mathbf{x}_n | \mathbf{X}_{n-1,i}^A)$

Measurement weights: $w_{u,n,i,j}^M = f_{Y_{u,n}|X_{u,n}}(y_{u,n}^* | X_{u,n,i,j}^P)$

Adapted resampling weights: $w_{n,i,j}^A = \prod_{u=1}^U w_{u,n,i,j}^M$

Resampling: $\mathbb{P}[r(i) = a] = w_{n,i,a}^A \left(\sum_{k=1}^J w_{n,i,k}^A \right)^{-1}$

$\mathbf{X}_{n,i}^A = \mathbf{X}_{n,i,r(i)}^P$

Compute $\gamma_{u,n+k,i,k}$ for k in $0:K$,

Compute $\gamma_{u,n,i,0}^+$

End for

$$\ell_{u,n}^{\text{MC}} = \log \left(\frac{\sum_{i=1}^{\mathcal{I}} \gamma_{u,n,i,0}^+ \prod_{k=1}^K \gamma_{u,n,i,k}}{\sum_{i=1}^{\mathcal{I}} \prod_{k=0}^K \gamma_{u,n,i,k}} \right)$$

It is clearer from the ABF₂ representation than from the ABF₁ representation that we do not have to save every individual particle and its weight $w_{u,n,i,j}^M$ after the quantities $\mathbf{X}_{n,i}^A$, $\gamma_{u,n+k,i,k}$ and $\gamma_{u,n,i,0}^+$ have been computed. ABF₂ has an embarrassingly parallel implementation, since the replicates do not need to interact until they are combined to compute $\ell_{u,n}^{\text{MC}}$. An embarrassingly parallel implementation therefore requires $O(U(KN + J))$ memory for each replicate, and $O(UNLK)$ memory when the results from each replicate are collected together.

By using additional communication, for example when the implementation is designed for a single core or multiple cores with shared memory, it is possible to further reduce the memory requirement. At time n , we need to save only $\mathbf{X}_{n,i}^A$ and $\gamma_{u,n-K:n+K,i,k}$ to compute $\ell_{u,n}^{\text{MC}}$ and all subsequent quantities. Computing $\mathbf{X}_{n,i}^A$ requires $O(UJ)$ storage. Therefore, ABF can be implemented with memory requirement $O(U(K\mathcal{I} + J))$, independent of N .

S10 Bagged filters for functions of the latent states

The theory and methodology in the main article focused on filtering for likelihood estimation. Here, we describe extensions to other filtering problems. Let $\{\phi_k : \mathbf{X}^U \rightarrow \mathbb{R}, k \text{ in } 1:K\}$ be a collection of functions where ϕ_k depends only on a subset of units $\Phi_k \subset 1:U$. We suppose that there exist neighborhoods

$$B'_{k,n} \subset A'_n = (1:U) \times (0:n) \tag{S60}$$

such that $\phi_k(\mathbf{X}_n)$ is approximately independent of $\{Y_{u,n} : (u,n) \in B'_{k,n}\}$ given $\{Y_{u,n} : (u,n) \in B'_{k,n}\}$, where $B'_{k,n}$ is a complement in A'_n . Unlike the sets $A_{u,n}$ and $B_{u,n}$ defined for likelihood estimation, the sets A'_n and $B'_{k,n}$ can include any locations at time n . We consider Monte Carlo estimation of

$$\bar{\phi}_{k,n} = \mathbb{E}[\phi_k(\mathbf{X}_n) | \mathbf{Y}_{1:n}], \quad k \text{ in } 1:K. \tag{S61}$$

For example, if we set $\phi_u(\mathbf{x}_n) = x_{u,n}$ and $K = U$, the collection of quantities $\{\bar{\phi}_{u,n}\}$ estimated in (S61) corresponds to a vector of filter means. Setting $\phi_k(\mathbf{x}_n) = x_{u_k,n} x_{\tilde{u}_k,n}$ enables calculation of a collection of filter covariances between units u_k and \tilde{u}_k for k in $1:K$.

We consider bagged filtering approaches to estimation of $\{\bar{\phi}_{k,n}, k \text{ in } 1:K\}$. Although each $\bar{\phi}_{k,n}$ is required to have only local dependence, some global quantities such as filter means and

their variances across all units, can be expressed in terms of collections of such quantities. For bagged filtering to operate successfully, the neighborhoods $\{B'_{k,n}\}$ should not be large. Since $B'_{k,n}$ will typically be larger than $\{\Phi_k\}$, this rules out estimation of filtered quantities that cannot be adequately represented by a collection of localized filtering calculations. We now present variants of the pseudocode in the main text, targeted at estimation of $\{\bar{\phi}_{k,n}, k \text{ in } 1:K\}$. We do not prove theorems about these algorithms, but we conjecture from their similarity to the algorithms in the main text that comparable theoretical results should exist. Table S-5 lists the inputs, outputs and ranges of the implicit loops for the following algorithms.

Latent state estimation via bagged filters.

input:
collection of functions, ϕ_k
neighborhoods, $B'_{k,n}$
simulator for $f_{\mathbf{X}_0}(\mathbf{x}_0)$ and $f_{\mathbf{X}_n|\mathbf{X}_{n-1}}(\mathbf{x}_n | \mathbf{x}_{n-1})$
evaluator for $f_{Y_{u,n}|X_{u,n}}(y_{u,n} | x_{u,n})$
number of replicates, \mathcal{I}
data, $\mathbf{y}_{1:N}^*$
ABF and ABF-IR: particles per replicate, J
ABF-IR: number of intermediate timesteps, S
ABF-IR: measurement variance parameterizations, $\overleftarrow{v}_{u,n}$ and $\overrightarrow{v}_{u,n}$
ABF-IR: approximate process and observation mean functions, $\boldsymbol{\mu}$ and $h_{u,n}$

output:
filter estimate, $\bar{\phi}_{k,n}^{\text{MC}}$

implicit loops:
 u in $1:U$, n in $1:N$, i in $1:\mathcal{I}$, j in $1:J$, k in $1:K$

Table S-5: Notation for bagged filter for latent state estimation: inputs, outputs and implicit loops.

UBF. Unadapted bagged filter for latent state estimation.

Simulate $\mathbf{X}_{0:N,i} \sim f_{\mathbf{X}_{0:N}}(\mathbf{x}_{0:N})$

Measurement weights, $w_{u,n,i}^M = f_{Y_{u,n}|X_{u,n}}(y_{u,n}^* | X_{u,n,i})$

Filtering weights, $w_{k,n,i}^F = \prod_{(\tilde{u}, \tilde{n}) \in B'_{k,n}} w_{\tilde{u}, \tilde{n}, i}^M$

$$\bar{\phi}_{k,n}^{\text{MC}} = \frac{\sum_{i=1}^{\mathcal{I}} \phi_k(\mathbf{X}_{n,i}) w_{k,n,i}^F}{\sum_{i=1}^{\mathcal{I}} w_{k,n,i}^F}$$

ABF. Adapted bagged filter for latent state estimation.

Initialize adapted simulation: $\mathbf{X}_{0,i}^A \sim f_{\mathbf{X}_0}(\mathbf{x}_0)$

For n in $1:N$

Proposals: $\mathbf{X}_{n,i,j}^P \sim f_{\mathbf{X}_n | X_{1:U,n-1}}(\mathbf{x}_n | \mathbf{X}_{n-1,i}^A)$

Measurement weights: $w_{u,n,i,j}^M = f_{Y_{u,n}|X_{u,n}}(y_{u,n}^* | X_{u,n,i,j}^P)$

Adapted resampling weights: $w_{n,i,j}^A = \prod_{u=1}^U w_{u,n,i,j}^M$

Resampling: $\mathbb{P}[r(i) = a] = w_{n,i,a}^A \left(\sum_{q=1}^J w_{n,i,q}^A \right)^{-1}$

$\mathbf{X}_{n,i}^A = \mathbf{X}_{n,i,r(i)}^P$

$$w_{k,n,i,j}^F = \prod_{\tilde{n}=1}^{n-1} \left[\frac{1}{J} \sum_{q=1}^J \prod_{\tilde{u}: (\tilde{u}, \tilde{n}) \in B'_{k,n}} w_{\tilde{u}, \tilde{n}, i, q}^M \right] \prod_{\tilde{u}: (\tilde{u}, n) \in B'_{k,n}} w_{\tilde{u}, n, i, j}^M$$

End for

$$\bar{\phi}_{k,n}^{\text{MC}} = \frac{\sum_{i=1}^{\mathcal{I}} \sum_{j=1}^J \phi_k(\mathbf{X}_{n,i,j}^P) w_{k,n,i,j}^F}{\sum_{i=1}^{\mathcal{I}} \sum_{j=1}^J w_{k,n,i,j}^F}$$

**ABF-IR. Adapted bagged filter with intermediate resampling
for latent state estimation.**

Initialize adapted simulation: $\mathbf{X}_{0,i}^A \sim f_{\mathbf{X}_0}(\mathbf{x}_0)$

For n in $1:N$

Guide simulations: $\mathbf{X}_{n,i,j}^G \sim f_{\mathbf{X}_n|\mathbf{X}_{n-1}}(\mathbf{x}_n | \mathbf{X}_{n-1,i}^A)$

Guide sample variance: $V_{u,n,i} = \text{Var}\{h_{u,n}(X_{u,n,i,j}^G), j \text{ in } 1:J\}$

$g_{n,0,i,j}^R = 1$ and $\mathbf{X}_{n,0,i,j}^{\text{IR}} = \mathbf{X}_{n-1,i}^A$

For s in $1:S$

Intermediate proposals: $\mathbf{X}_{n,s,i,j}^{\text{IP}} \sim f_{\mathbf{X}_{n,s}|\mathbf{X}_{n,s-1}}(\cdot | \mathbf{X}_{n,s-1,i,j}^{\text{IR}})$

$\boldsymbol{\mu}_{n,s,i,j}^{\text{IP}} = \boldsymbol{\mu}(\mathbf{X}_{n,s,i,j}^{\text{IP}}, t_{n,s}, t_n)$

$V_{u,n,s,i,j}^{\text{meas}} = \vec{v}_u(\theta, \boldsymbol{\mu}_{u,n,s,i,j}^{\text{IP}})$

$V_{u,n,s,i}^{\text{proc}} = V_{u,n,i}(t_n - t_{n,s}) / (t_n - t_{n,0})$

$\theta_{u,n,s,i,j} = \overleftarrow{v}_u(V_{u,n,s,i,j}^{\text{meas}} + V_{u,n,s,i}^{\text{proc}}, \boldsymbol{\mu}_{u,n,s,i,j}^{\text{IP}})$

$g_{n,s,i,j} = \prod_{u=1}^U f_{Y_{u,n}|X_{u,n}}(y_{u,n}^* | \boldsymbol{\mu}_{u,n,s,i,j}^{\text{IP}}; \theta_{u,n,s,i,j})$

Guide weights: $w_{n,s,i,j}^G = g_{n,s,i,j} / g_{n,s-1,i,j}^R$

Resampling: $\mathbb{P}[r(i,j) = a] = w_{n,s,i,a}^G \left(\sum_{q=1}^J w_{n,s,i,q}^G \right)^{-1}$

$\mathbf{X}_{n,s,i,j}^{\text{IR}} = \mathbf{X}_{n,s,i,r(i,j)}^{\text{IP}}$ and $g_{n,s,i,j}^R = g_{n,s,i,r(i,j)}$

End For

Set $\mathbf{X}_{n,i}^A = \mathbf{X}_{n,S,i,1}^{\text{IR}}$

Measurement weights: $w_{u,n,i,j}^M = f_{Y_{u,n}|X_{u,n}}(y_{u,n}^* | X_{u,n,i,j}^G)$

$$w_{k,n,i,j}^F = \prod_{\tilde{n}=1}^{n-1} \left[\frac{1}{J} \sum_{q=1}^J \prod_{\tilde{u}: (\tilde{u}, \tilde{n}) \in B'_{k,n}} w_{\tilde{u}, \tilde{n}, i, q}^M \right] \prod_{\tilde{u}: (\tilde{u}, n) \in B'_{k,n}} w_{\tilde{u}, n, i, j}^M$$

End for

$$\bar{\phi}_{k,n}^{\text{MC}} = \frac{\sum_{i=1}^{\mathcal{I}} \sum_{j=1}^J \phi_k(\mathbf{X}_{n,i,j}^{\text{P}}) w_{k,n,i,j}^F}{\sum_{i=1}^{\mathcal{I}} \sum_{j=1}^J w_{k,n,i,j}^F}$$

S11 An iterated bagged filter for parameter estimation

This paper focuses on evaluating the likelihood function for SpatPOMP models via filtering. Although the likelihood function is fundamental for inference, evaluation alone is not sufficient. Likelihood maximization enables calculation of the maximum likelihood estimate, profile likelihood confidence intervals, likelihood ratio tests and likelihood-based model selection criteria. Iterated filtering methodology (Ionides et al., 2006, 2011, 2015) provides an approach to extending filtering algorithms to likelihood maximization algorithms. Here, we demonstrate one such extension in the context of bagged filters. This demonstration provides a proof of concept to motivate future work.

Iterated filtering approaches apply filtering to a modified version of the model where parameters are perturbed at each time point. The filtering procedure directs the perturbed parameters toward values consistent with the data. At the end of each filtering operation, a parameter updating rule is applied and a new filtering iteration is started with reduced perturbation variance. Under suitable conditions, iterative procedures of this type converge to a neighborhood of a maximum likelihood

Table S-6: Iterated bagged filter inputs, outputs and implicit loops, extending ABF table in main text.

input: same as ABF table in main text plus
Number of maximization iterations, M
Number of parameter vectors, K
Perturbation variance, Σ
Variance reduction factor after 50 iterations, α
Starting parameters, $\theta_{1:K}^{(0)}$
Resampling proportion, p
output:
Parameter estimates approaching the maximum likelihood estimate, $\theta_{1:K}^{(M)}$
implicit loop:
k in $1:K$, i in $1:\mathcal{I}$

parameter despite the presence of Monte Carlo filtering error. We implemented an iterated bagged filter procedure, described by the pseudocode below. The pseudocode is presented for an iterated adapted bagged filter (IABF) but the iterated unadapted filter (IUBF) corresponds to the case $J = 1$ and the iterated bagged filter with intermediate resampling (IABF-IR) follows by adding the intermediate resampling procedure used by ABF-IR. The filtering step of IABF uses ABF to estimate the likelihood at the K perturbed parameter sets. The selection step does not resample parameters based on these estimated likelihood. Rather, it selects the parameters with the top p quantile of likelihoods and copies them appropriately to get K new parameters for the next filtering step. This quantile-based resampling allows us to maintain the diversity of the K parameter sets and avoid *parameter degeneracy*, whereby very few parameters are resampled, leading to an inefficient search of parameter space.

For simplicity, in this description, we assume that parameters are transformed so that their values are unconstrained. Our software implementation, provided the R package `spatPomp` (Asfaw et al., 2021), provides facilities for carrying out such transformations. The Gaussian distribution used for perturbations, and the geometric perturbation variance reduction factor, α , are convenient specifications but are not required in theory (Ionides et al., 2015). As another simplification, the pseudocode for IABF represents the logical structure of the algorithm without attending to issues of memory management and parallelization. For implementation issues, we refer to `spatPomp` (Asfaw et al., 2021).

In Figure 5 of the main text, we use this IABF implementation to construct a profile likelihood for the measles model. We use $J = 1$, $\mathcal{I} = 30000$, $K = 250$, $p = 0.8$, $\alpha = 0.5$, $M = 15$ and Σ set to be a diagonal matrix with perturbation variance for each non-initial value parameter set to 0.02. For this exercise, we fix the initial value parameters at their true values.

The resulting Monte Carlo parameter estimates have Monte Carlo uncertainty in both likelihood evaluation and maximization. Therefore, we used a Monte Carlo adjusted profile likelihood (Ionides et al., 2017; Ning et al., 2021) that accounts for this uncertainty. Fig. 5 gives empirical demonstration of this procedure on the measles model.

IABF. Iterated adapted bagged filter.

For m in $1:M$

$$\theta_{0,1:K}^F = \theta_{1:K}^{(m-1)}$$

Initialize adapted simulation: $\mathbf{X}_{0,i,k}^F \sim f_{\mathbf{X}_0}(\mathbf{x}_0; \theta_{0,k}^F)$

For n in $1:N$

$$\theta_{n,k}^P \sim \mathcal{N}[\theta_{n-1,k}^F, \alpha^{2m/50}\Sigma]$$

$$\mathbf{X}_{n,i,j,k}^P \sim f_{\mathbf{X}_n|\mathbf{X}_{n-1}}(\mathbf{x}_n | \mathbf{X}_{n-1,i,k}^F; \theta_{n,k}^P)$$

$$\text{Measurement weights: } w_{u,n,i,j,k}^M = f_{Y_{u,n}|X_{u,n}}(y_{u,n}^* | X_{u,n,i,j,k}^P; \theta_{n,k}^P)$$

$$\text{Adapted resampling weights: } w_{n,i,j,k}^A = \prod_{u=1}^U w_{u,n,i,j,k}^M$$

$$\text{State resampling: } \mathbb{P}[r(i,k) = a] = w_{n,i,a,k}^A \left(\sum_{\xi=1}^J w_{n,i,\xi,k}^A \right)^{-1}$$

$$\mathbf{X}_{n,i,k}^A = \mathbf{X}_{n,i,r(i,k),k}^P$$

$$w_{u,n,i,j,k}^P = \prod_{\tilde{n}=1}^{n-1} \left[\frac{1}{J} \sum_{\xi=1}^J \prod_{\tilde{u}:(\tilde{u},\tilde{n}) \in B_{u,n}} w_{\tilde{u},\tilde{n},i,\xi,k}^M \right] \prod_{\tilde{u}:(\tilde{u},n) \in B_{u,n}} w_{\tilde{u},n,i,j,k}^M$$

$$\ell_{n,k}^{\text{MC}} = \sum_{u=1}^U \log \left(\frac{\sum_{i=1}^{\mathcal{I}} \sum_{j=1}^J w_{u,n,i,j,k}^M w_{u,n,i,j,k}^P}{\sum_{i=1}^{\mathcal{I}} \sum_{j=1}^J w_{u,n,i,j,k}^P} \right)$$

Select the highest pK likelihoods: find s with

$$\{s(1), \dots, s(\lceil pK \rceil)\} = \{k : \sum_{k=1}^K \mathbf{1}\{\ell_{n,k}^{\text{MC}} > \ell_{n,k}^{\text{MC}}\} < (1-p)K\}$$

Make $1/p$ copies of successful parameters, $\theta_{n,k}^F = \theta_{n,s(\lceil pk \rceil)}^P$

$$\mathbf{X}_{n,i,k}^F = \mathbf{X}_{n,i,s(\lceil pk \rceil)}^A$$

End for

$$\theta_k^{(m)} = \theta_{N,k}^F$$

End for

S12 Replicates versus particles for the measles model

It is necessary in practice to decide whether computational resources are best directed toward a large number of replicates, \mathcal{I} , or a large number of particles per replicate, J . Computational effort for ABF and ABF-IR is approximately proportional to $J\mathcal{I}$, and UBF corresponds to ABF with $J = 1$. Suitable algorithmic parameters may depend on the model under consideration, and here we consider resource allocation for the measles model studied in the main text, using simulated data with $U = 40$ and $N = 104$. From Figure 4, we know that this implementation of the model is well suited to ABF and UBF. ABF-IR performs less well, and the weak performance of GIRF suggests that the weakness may be due to an inadequate guide function. Figure S-5 investigates the tradeoff between UBF and ABF by plotting evaluated log likelihood against \mathcal{I} with J chosen to give approximately a constant computational effort. Algorithmic settings and run times are reported in Table S-7. For our implementation, choosing J very low and \mathcal{I} correspondingly high led to greater computation time, perhaps because the code was written to parallelize nicely when J is relatively large.

We interpret the bimodal curve as follows. When ABF is carried out with an inadequate number of particles for each bootstrap replicate, the algorithm cannot make a good representation of a draw from the adapted distribution. In that case, there is an advantage to using UBF, which does not attempt to carry out adapted simulation. For very small numbers of particles per replicate, the ABF

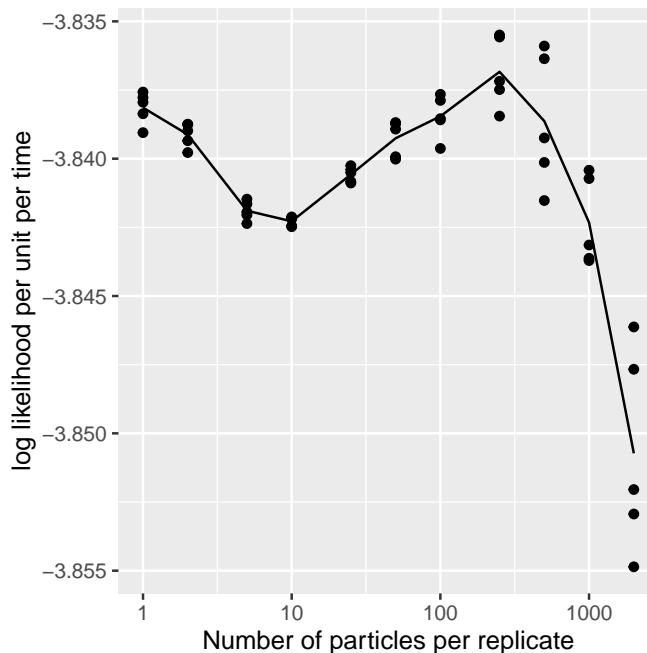


Figure S-5: log likelihood estimates for simulated data from the measles model using ABF, with varying algorithmic parameters.

algorithm behaves like a not-quite-properly-weighted version of UBF. Large numbers of particles per replicate presumably lead to improved Monte Carlo representation of draws from the adapted distribution, but computational cost constraints prevent combining this with a large number of replicates. We see a mode around 500 particles per replicate where ABF out-performs UBF. On this problem, UBF is relatively successful, presumably because the measles dynamics in each city are strongly attracted toward relatively few stable cycles (annual epidemics, or peaks in odd years, or peaks in even years) and a tractable number of simulations can represent all these scenarios. The Lorenz model of Sec. S8 provides an alternative situation, where adaptation has more advantages. Also, the plug-and-play guide function appears to operate successfully in this case, as evidenced by relatively strong performance from ABF-IR and GIRF.

J	\mathcal{I}	time
2000	500	70.7
1000	1000	71.3
500	2000	72.4
250	4000	75.0
100	10000	80.9
50	20000	93.8
25	40000	114.9
10	40000	71.4
5	40000	56.1
2	40000	47.7
1	40000	43.0

Table S-7: Bootstrap replications, \mathcal{I} , particles per replicate, J , and computational time (total minutes for the five points) for the results presented in Figure S-5

Supplementary References

- Ades, M. and Van Leeuwen, P. J. (2015). The equivalent-weights particle filter in a high-dimensional system. *Quarterly Journal of the Royal Meteorological Society*, 141(687):484–503.
- Asfaw, K., Park, J., Ho, A., King, A. A., and Ionides, E. L. (2021). Statistical inference for spatiotemporal partially observed Markov processes via the R package spatpomp. *arXiv:2101.01157*.
- Evensen, G. and van Leeuwen, P. J. (1996). Assimilation of geostat altimeter data for the Agulhas Current using the ensemble Kalman filter with a quasigeostrophic model. *Monthly Weather Review*, 124:58–96.
- Ionides, E. L., Bhadra, A., Atchadé, Y., and King, A. A. (2011). Iterated filtering. *Annals of Statistics*, 39:1776–1802.
- Ionides, E. L., Bretó, C., and King, A. A. (2006). Inference for nonlinear dynamical systems. *Proceedings of the National Academy of Sciences of the USA*, 103:18438–18443.
- Ionides, E. L., Breto, C., Park, J., Smith, R. A., and King, A. A. (2017). Monte Carlo profile confidence intervals for dynamic systems. *Journal of the Royal Society Interface*, 14:1–10.
- Ionides, E. L., Nguyen, D., Atchadé, Y., Stoev, S., and King, A. A. (2015). Inference for dynamic and latent variable models via iterated, perturbed Bayes maps. *Proceedings of the National Academy of Sciences of the USA*, 112(3):719—724.
- Liu, J. S. (2001). *Monte Carlo Strategies in Scientific Computing*. Springer, New York.
- Lorenz, E. N. (1996). Predictability: A problem partly solved. *Proceedings of the Seminar on Predictability*, 1:1–18.
- Ning, N., Ionides, E. L., and Ritov, Y. (2021). Scalable Monte Carlo inference and rescaled local asymptotic normality. *Bernoulli*, pre-published online.
- Park, J. and Ionides, E. L. (2020). Inference on high-dimensional implicit dynamic models using a guided intermediate resampling filter. *Statistics & Computing*, 30:1497–1522.
- van Kekem, D. L. and Sterk, A. E. (2018). Travelling waves and their bifurcations in the Lorenz-96 model. *Physica D: Nonlinear Phenomena*, 367:38–60.